# LONG DURATION EXPOSURE FACILITY (LDEF) EXPERIMENT M0003 METEOROID AND DEBRIS SURVEY

M. J. Meshishnek, S. R. Gyetvay, K. W. Paschen, and J. M. Coggi
Mechanics and Materials Technology Center
The Aerospace Corporation
El Segundo, CA 90245-4691
Phone: 310/336-8760, Fax: 310/336-1636

## SUMMARY

A survey of the meteoroid and space debris impacts on LDEF experiment M0003 has been performed. The purpose of this survey was to document significant impact phenomenology and to obtain impact crater data for comparison to current space debris and micrometeoroid models. The survey consists of photomicrographs of significant impacts in a variety of material types; accurate measurements of impact crater coordinates and dimensions for selected experiment surfaces, and databasing of the crater data for reduction, manipulation, and comparison to models. Large area surfaces that were studied include the experiment power and data system (EPDS) sunshields, environment exposure control canister (EECC) sunshields, and the M0003 signal conditioning unit (SCU) covers. Crater diameters down to 25 microns were measured and catalogued. Both leading (D8) and trailing (D4) edge surfaces were studied and compared. The EPDS sunshields are aluminum panels painted with Chemglaze A-276 white thermal control paint, the EECC sunshields are chromic acid-anodized aluminum, and the SCU covers are aluminum painted with S13GLO white thermal control paint. Typical materials that have documented impacts are metals, glasses and ceramics, composites, polymers, electronic materials, and paints. The results of this survey demonstrate the different response of materials to hypervelocity impacts. Comparison of the survey data to curves derived from the Kessler debris model and the Cour-Palais micrometeoroid model indicates that these models overpredict small impacts (< 100 micron) and may underpredict large impacts (> 1000 micron) while having fair to good agreement for the intermediate impacts. Comparison of the impact distributions among the various surfaces indicates significant variations, which may be a function of material response effects, or in some cases surface roughness. Representative photographs and summary graphs of the impact data are presented.

## I. INTRODUCTION

The successful retrieval of the Long Duration Exposure Facility (LDEF) has provided a unique opportunity for the study of micrometeoroid and debris impacts. Originally intended for an 11-month mission, LDEF remained in orbit for nearly six years (69 months). This extended stay in space significantly increased the value of LDEF for the study of micrometeoroid and space debris phenomena. Due to its gravity gradient stabilized attitude, LDEF had each of its surfaces in a constant and known orientation with respect to its velocity vector. Thus, a study of the impacts on various surfaces of LDEF should provide information with respect to the spatial and angular distribution of impactors and provide information on both space debris and micrometeoroid impacts. The large number of impacts observed on LDEF enables meaningful comparisons of this data to current models used for the prediction of such events. In addition, the large number of material types flown on LDEF provides startling examples of various materials' responses to hypervelocity phenomena. Comparison of observed impact damage with laboratory simulations should

also prove fruitful. For these reasons, the LDEF Meteoroid and Debris Special Investigation Group performed extensive examinations of all LDEF experiments and hardware during the deintegration process at KSC.[1]

The Aerospace Corporation LDEF experiment (SSD-802/M0003) housed in four of the 86 LDEF trays and positioned on the leading and trailing edges of the LDEF structure contained well over 1200 samples of over 200 material types. Many of these materials had essentially identical samples on the leading and trailing edges. Moreover, the experiment had some relatively large area sunshields, which provided prime surfaces for impact counts. For these reasons, a meteoroid and debris survey of M0003 was undertaken with the objectives of documenting the impact phenomenology and impact crater statistics.

## II. BACKGROUND

The LDEF is a NASA satellite designed to study the effects of prolonged exposure to the space environment. Experiments carried aloft on LDEF numbered 57 and were from the following four categories: materials, coatings and thermal systems; electronics and optics; power and propulsion; and science. These experiments were housed in 86 experiment trays attached to the LDEF structure. The LDEF itself is a dodecahedral cylindrical framework with spaces for 72 trays on the circumference; the remaining 8 and 6 trays are mounted on the space- and earth-facing ends of the structure. The LDEF was designed to orbit the earth in fixed orientation due to gravity gradient stabilization. This three-axis stabilization caused LDEF to have one end pointed toward the earth and the other towards space. Furthermore, one side of LDEF, called the leading edge, was always normal to the velocity vector, while another side, known as the trailing edge, was always in the spacecraft wake. The LDEF was equipped with a viscous magnetic dampener to reduce or eliminate oscillation of the spacecraft. Figure II-1 depicts the LDEF structure together with the numbering
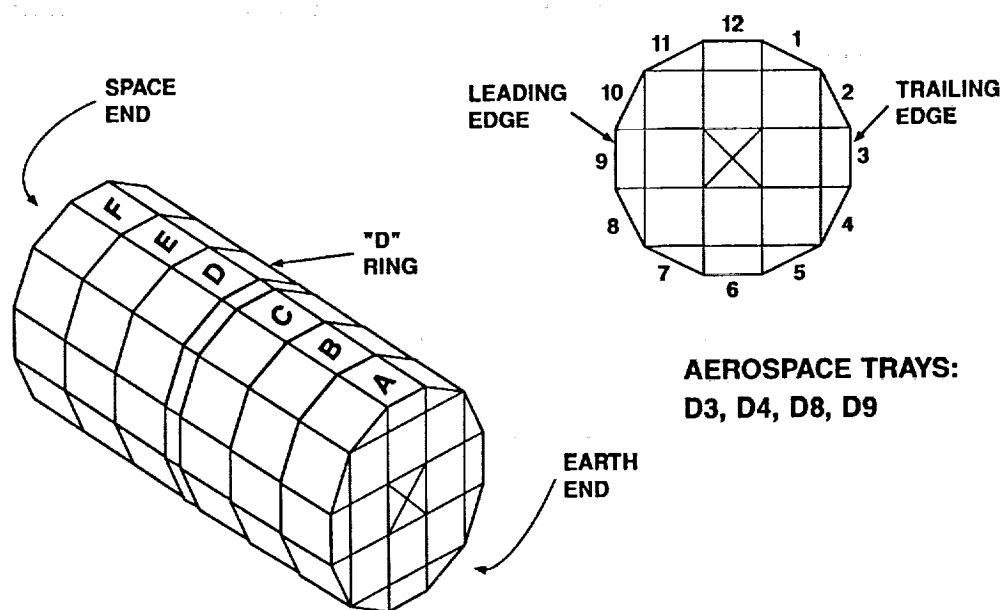


Figure II-1. LDEF surface nomenclature.

scheme for the tray positions and the nomenclature for the various faces of the spacecraft. It is important to realize that, due to its unique structure and orientation, the environment around LDEF varies with location. The principal differences in the environment are the concentration of atomic oxygen, which is highest on the leading edge and diminishes to zero on the trailing edge, and the much larger number of impactors that hit the leading versus the trailing edge of LDEF.[2]

LDEF was deployed on STS mission 41C on 7 April 1984 and was originally intended for an 11- month mission. However, due to problems encountered with the Shuttle schedule and the ensuing Challenger disaster, LDEF was not retrieved until 12 Jan. 1990. This allowed LDEF to remain in orbit for 69 months, increasing by over a factor of six the time during which the spacecraft would encounter micrometeoroids and space debris. During this time, the orbit of LDEF decayed, descending from the deployment altitude of 257 nmi to 179 nmi at retrieval. However, the orientation of LDEF remained stable during this period. The decrease in altitude produced changes in the environment surrounding LDEF, most notably the density of atomic oxygen and the concentration of meteoroids and debris. At the lower altitude, the concentration of atomic oxygen rises dramatically, while the density of meteoroids and debris decreases slightly.[2]

A significant amount of work has been performed by the LDEF Meteoroid and Debris Special Investigation Group and other LDEF experimenters in documenting, analyzing, and modeling the vast number of hypervelocity impacts that occurred on LDEF.[3-11] These hypervelocity impact features are produced by collisions between space debris particles or dust and small meteoroids with spacecraft surfaces. Collision velocities can vary widely and depend upon the constant orbital velocity of the earth, the spacecraft orbital velocity, the impactor velocity, and the direction of impact. The collision velocities for space debris particles range from about 3 to 15 km/s, with average values of 10 to 13 km/s. The distribution of velocities has been given by Kessler.[12] For meteoroids, the collision velocities range from about 3 to 72 km/s with an average velocity of 19 km/s. Zook and Erickson have provided data that give the distribution of meteoroid velocities seen by spacecraft.[11,13-15]

With respect to hypervelocity impacts in materials, different phenomena are observed depending on the impact velocity, relative sizes of the impactor and target, and material properties of the target. For targets that are thick relative to impactor sizes, craters will be formed that generally have lips resulting from plastic flow to molten spatter. However, for very thin targets, such as foils, which are much smaller than the impactor diameter, perforations occur resulting in a hole only slightly larger than the impactor diameter. Secondary or collateral damage can occur from the impactor remnants and the punched-out section. For high-velocity impacts, both the target foil and the impactor are vaporized. However, for lower velocities, the impactor and foil can remain molten or solid, and collateral damage is possible.

Brittle materials, such as glasses or ceramics, often have chonchoidal surface spalls and cracks, and may have star cracks propagating radially from the crater. Layered targets, such as coated substrates, often exhibit delamination around or near the crater. If one averages all impacts, the ratio of crater size to impactor size is generally about 5. For local spall regions, the spall radius to impactor radius ratio is about 20. Star cracks, when formed, can extend outward over 100 times the impactor diameter.

## III. EXPERIMENT DESCRIPTION

One of the most comprehensive materials experiments on board LDEF, M0003, was integrated by The Aerospace Corporation Materials Sciences Laboratory as Principal Investigator, and was designed to study the effects of the space environment on current and developmental spacecraft materials. Assembled on two leading-edge and two trailing-edge trays that contained over 1274 specimens, two active data systems, and two timed exposure vacuum canisters, the experiment was a collection of 19 subexperiments from The Aerospace Corporation Laboratories, Air Force and Navy Laboratories, and Department of Defense Contractors. Many of these materials are currently in use on Space and Missile Systems Center (SMC) spacecraft. The Aerospace Corporation, as the integrating agency, was charged with the documentation of the experiment from the earliest stages of retrieval through the complete deintegration of the trays. This included detailed examination and photography of the individual specimens during removal and packaging. Special attention was given to documentation of meteoroid and debris impact phenomenology. Additionally, several surfaces of the experiment hardware, such as the sunshields for the data systems and canisters, were examined in great detail for the size and number of impacts as well as their material response. These surfaces provided large areas for study (> 1.5 m$^2$) and, therefore, statistically large numbers of craters to count. The surfaces studied were on the leading-edge tray, D8, and the trailing-edge tray, D4. They are referred to as "leading edge" for D8 and "trailing edge" for D4 for simplicity. However, since the leading and trailing edges of LDEF were rows 9 and 3, respectively, it must be recognized that the surfaces in this study were actually 30° off-normal to the leading and trailing edges. Moreover, measurements made on the LDEF and the results from some experiments have determined that the LDEF structure was actually off normal alignment with the velocity vector by about 8°.[16] Thus, tray D8 was 38° from normal to the velocity vector or ram.

The immediate objectives of the experiment were to understand the changes in the structure and properties of materials resulting from exposure to the natural space environment and to compare them to predictions based on laboratory experiments. Ideally, correlation of changes in physical properties will be made with changes in microstructure. The longer-term objectives were to improve the performance and usage of existing materials and to decrease the lead times for application of new materials on DOD space systems. An important outcome expected from this experiment was the understanding and modeling of material degradation. Due to the longer exposure of LDEF to the space environment, the opportunity exists for a deeper and expanded study of material degradation due to meteoroid and debris impacts.

The M0003 experiment was a cooperative effort and provided the first opportunity for DOD space programs and laboratories to evaluate materials after long exposure to the space environment. From the recommendations of an advisory group composed of participating organizations, a mix of current and developmental spacecraft materials was chosen for this experiment. An overview of the material categories, the originating agency, and the Principal Investigator is given in Table I.

Table I. Summary of M0003 Experiments

| Subexperiment No. | Scope | Experimenter | Agency |
|---|---|---|---|
| -1 | Radar camouflage materials and electro-optical signature coatings | Richard Porter | Wright Labs/SNA, Wright Patterson AFB, OH 45433-6533 |
| -2 | Laser optics | Linda De Hainaut | Phillips Lab/LTC, Kirtland AFB, NM 87117-6008 |
| -3 | Structural materials | Charles Miglionico | Phillips Lab/SUE, Kirtland AFB, NM 87117-6008 |
| -4 | Solar power components | Terry Trumble | Wright Labs/POOC, Wright Patterson AFB, OH 45433-6533 |
| -5 | Thermal control materials | Charles Hurley | Univ. of Dayton Research Inst., 300 College Park, Dayton, OH 45469-0001 |
| -6 | Laser communication components | Randall R. Hodgson | McDonnell Douglas Astronautics Corp., Mail Code 1067267, P. O. Box 516,St. Louis, MO 63166 |
| -7 | Laser mirror coatings | Terry M. Donovan | Naval Weapons Center, Thin Film Physics Div. Code 3818, China Lake, CA 93555 |
| -8 | Composite materials, electronic piece parts, fiber optics | Gary Pippin | Boeing Aerospace Co., Materials technology Dept., MS 2E-01, P. O. Box J04, Sunnyvale, CA 94086 |
| -9 | Thermal control materials, antenna materials, composite materials, and cold welding | Brian C. Petrie | Lockheed Missiles & Space Co., Dept. 62-92, Bldg. 564, P. O. Box 92957, M2/321, Los Angeles, CA 90009 |
| -10 | Advanced composite materials | Gary L. Steckel | The Aerospace Corp., P. O. Box 92957, M2/321, Los Angeles, CA 90009 |
| -11, -12 | Contamination monitoring Radiation measurements | Eugene N. Borson | The Aerospace Corp., P. O. Box 92957, M2/250, Los Angeles, CA 90009 |
| -13 | Laser hardened materials | Randall R. Hodgson | McDonnell Douglas Astronautics Corp., Mail Code 1067267, P. O. Box 516,St. Louis, MO 63166 |
| -14 | Quartz crystal microbalance | Donald A. Wallace | QCM Research, 2825 Laguna Canyon Rd., P. O. Box 277, Laguna Beach, CA 92652 |
| -15 | Thermal control materials | Oscar Esquivel | The Aerospace Corp., P. O. Box 92957, M2/241, Los Angeles, CA 90009 |
| -16 | Advanced composites | Gary L. Steckel | The Aerospace Corp., P. O. Box 92957, M2/321, Los Angeles, CA 90009 |
| -17 | Radiation dosimetry | Sam S. Imamoto, J. Bernard Blake | The Aerospace Corp., P. O. Box 92957, M2/260, Los Angeles, CA 90009 |
| -18 | Thermal control paints | Christopher H. Jaggers | The Aerospace Corp., P. O. Box 92957, M2/271, Los Angeles, CA 90009 |
| -19 | Electronic piece parts | Seymour Feuerstein | The Aerospace Corp., P. O. Box 92957, M2/244, Los Angeles, CA 90009 |

The M0003 Experiment hardware consisted of four peripheral trays, two experiment power and data systems (EPDSs), two environment exposure control canisters (EECCs), two signal conditioning units (SCUs), and several Li/SO$_2$ batteries to provide experiment power. The experiment was an active one in that it was equipped to record temperature, strain, solar cell output, quartz crystal microbalance frequency, fiber optics output, circuit interrogation, and various data system parameters. One six-inch-deep tray and one

three-inch-deep tray connected by a wiring harness and containing a data system (EPDS), a canister (EECC), an SCU, and numerous material specimens were located on rows 8 and 9 of ring D on the leading edge of LDEF. A similar configuration was located on rows 3 and 4 of ring D on the trailing edge. The canisters were preprogrammed to provide timed exposures of specimens of 9, 19, and 40 weeks. The canisters closed after these exposure times had elapsed. The design of the trays was modular, allowing samples to be thermally coupled or decoupled from the tray and, therefore, the LDEF structure. Figures III-1 through III-4 illustrate the layout of the four trays, showing the location of the various components and sensors.

The test articles were mounted on black or clear anodized aluminum hardware modules within the trays. Most experiments had duplicate samples on both the leading and trailing edge trays; several had them in the canisters as well. Some experiments also included a set of control specimens that were reverse mounted on the modules, thereby exposing the samples only to thermal vacuum cycling. These test articles included a variety of thermal control coatings, optics, composites, structural materials, solar cells, fiber optics, laser communication components, antenna materials, electronic piece parts, dosimeters, and contamination monitors. The selection of sample complements, multiple locations, and flight controls increased the value and utility of the experiment by allowing differentiation of the environmental phenomena, especially those due to combined or synergistic effects. The most notable effects are the erosion of materials due to atomic oxygen and the impacts due to space debris. These two effects are prominent on the leading edge of LDEF and nearly absent on the trailing edge. Varying degrees of exposure provided by the canisters also aid in the study of these phenomena. Damage to the material samples is shown in the photos taken at Aerospace prior to deintegration of the trays (Figures III-5 through III-8). The damage and its impact on materials performance has been described previously.[17]
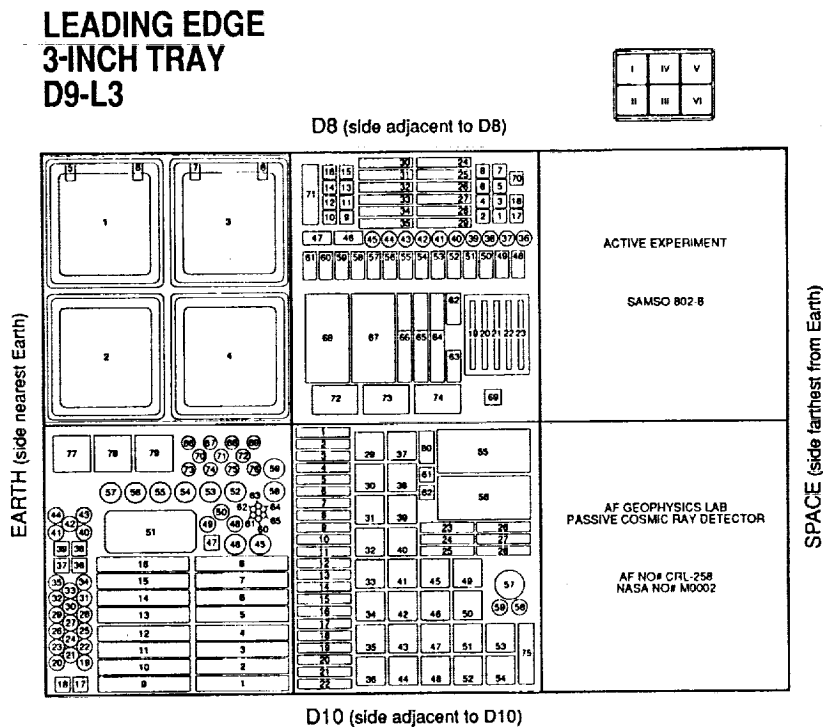


Figure III-1. Layout of D9 leading edge 3-inch-deep tray.

**TRAILING EDGE
3-INCH TRAY
D3-T3**

D2 (side adjacent to D2)

EARTH (side nearest Earth)

SPACE (side farthest from Earth)

PASSIVE EXPERIMENT

SAMSO 802-8

AF GEOPHYSICS LAB
PASSIVE COSMIC RAY DETECTOR

AF NO# CRL-258
NASA NO# M0002

D4 (side adjacent to D4)
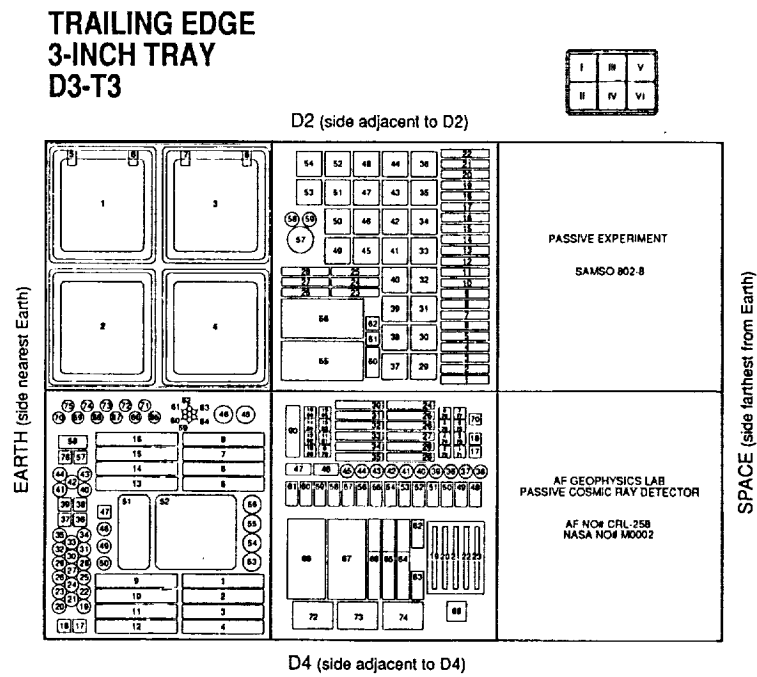
Figure III-2. Layout of D3 trailing edge 3-inch-deep tray.

**LEADING EDGE
6-INCH TRAY
D8-L6**

D7 (side adjacent to D7)

EARTH (side nearest Earth)

SPACE (side farthest from Earth)

E E C C
TRAY

SIGNAL
CONDITIONING
UNIT

12 VOLT
SYSTEM

7 5 VOLT
SYSTEM

E E C C
DRAWER
CONTROL

E E C C HOUSING

DATA PROCESSOR

TAPE RECORDER

D9 (side adjacent to D9)
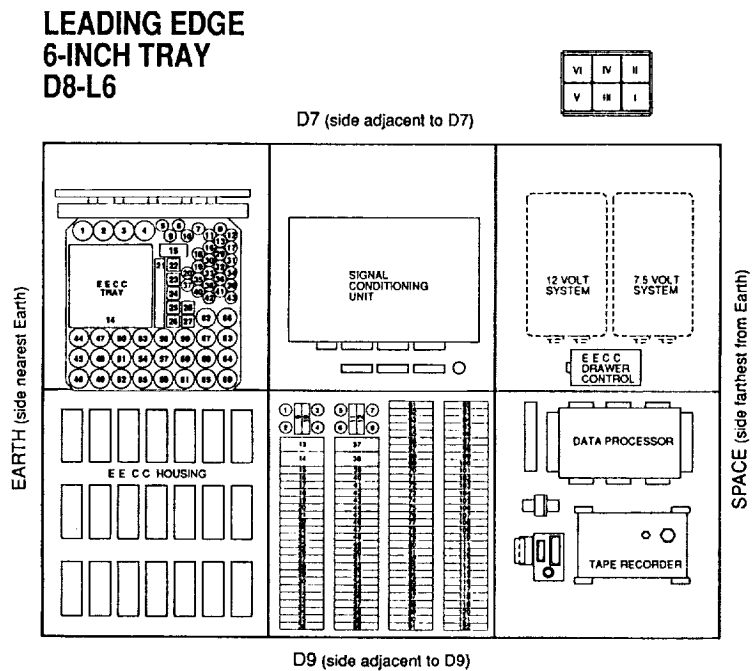
Figure III-3. Layout of D8 leading edge 6-inch-deep tray.

363

**TRAILING EDGE
6-INCH TRAY
D4-T6**

D3 (side adjacent to D3)
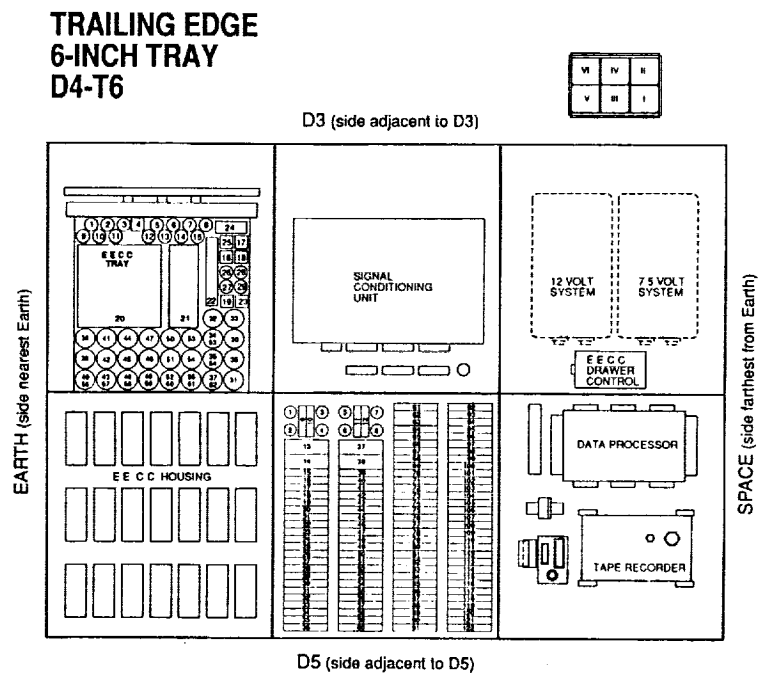
Figure III-4. Layout of D4 trailing edge 6-inch-deep tray.

Figure III-5. D9 tray postflight, prior to sample deintegration, in tray holding fixture.
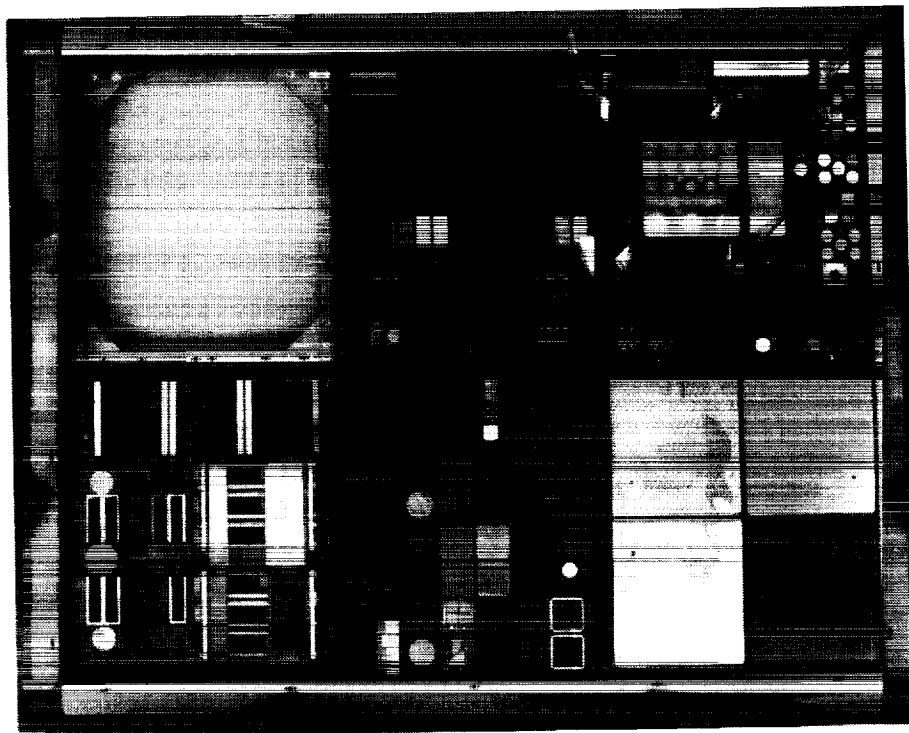
Figure III-6. D3 tray postflight, prior to sample deintegration, in tray holding fixture.



Figure III-7. D8 tray postflight, prior to sample deintegration, in tray holding fixture.
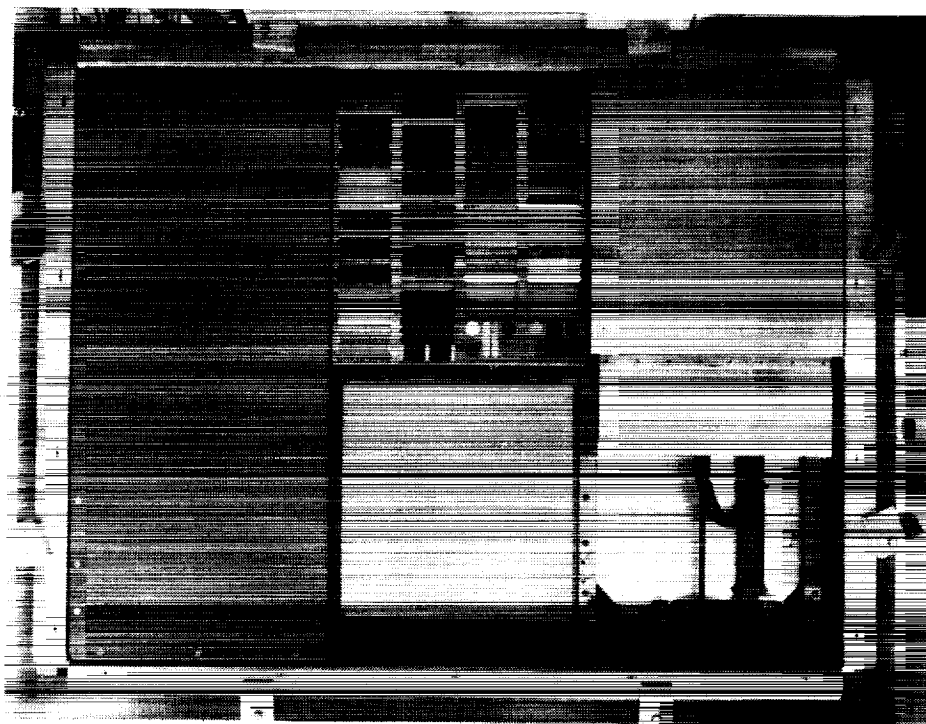
Figure III-8.  D4 tray postflight, prior to sample deintegration, in tray holding fixture.

## IV.  CRATER SURVEY METHOD

Documentation of the impacts on the various sunshields and covers was accomplished by manually scanning the panel with a 10X eyepiece mounted on an x-y translation system.  This fixture allowed determination of the crater's position and size.  Comparison to a reticule scale allowed measurement of the crater diameter. When possible, three measurements were made on each crater.  These corresponded to the actual crater diameter, the melt or spall zone surrounding the crater, and the larger area of delamination or damage.  These measurement conventions are shown in Figure IV-1.  All craters with diameters of 0.001 in. or greater (25 microns) were recorded.  In some cases, data was recorded on impacts where the only feature was the delamination zone of 0.001 in. to approximately 0.004 in.  However, data used for modeling consisted only of the craters with diameters 0.001 in. or greater.  This survey and the disassembly of the four LDEF trays were performed in a class 10,000 clean room facility at The Aerospace Corporation.  As the material specimens were removed from the trays, they were individually examined, preserving the orientation of the samples on LDEF. Each was photographed using brightfield, darkfield, and Nomarski optical microscopy techniques.  Typical micrometeoroid and debris damage was carefully photographed and documented.  In addition, crater counts were performed on the samples from subexperiment #2, Laser Optics, and subexperiment #19, Electronic

Materials. A Zeiss research microscope was used at 200X to 1000X, allowing observation of craters as small as 1 micron and as large as 782 microns on these samples. No perforations were observed.

A = Crater Diameter

B = Spall (melt) Zone

C = Delamination Zone
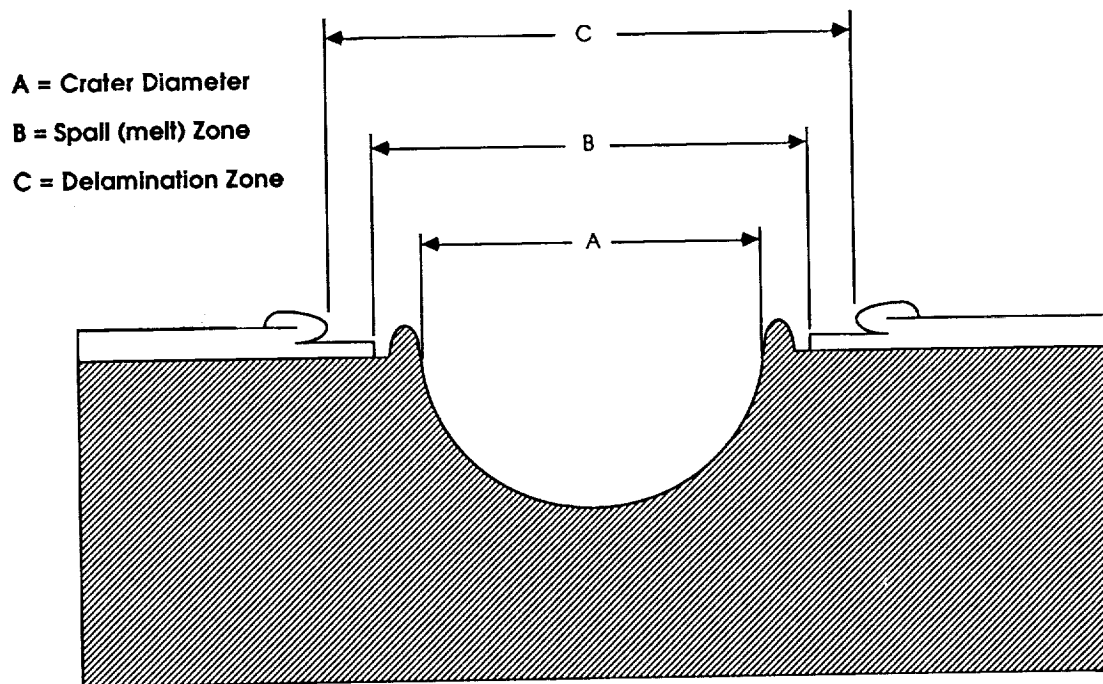
Figure IV-1. Micrometeoroid and debris survey terminology.

## V. RESULTS BY SAMPLE

Table II gives a brief synopsis of the surfaces surveyed in this study.

Table II. M0003 Surfaces Surveyed for M + D Damage.

| Designation | Substrate | Coating | LDEF Location | Observations |
|---|---|---|---|---|
| D8 EPDS Sunshield | Aluminum | Chemglaze A-276 | Leading edge, D8 | Chalky surface; AO eroded binder |
| D4 EPDS Sunshield | Aluminum | Chemglaze A-276 | Trailing edge, D4 | Dark brown; UV degraded binder |
| D8 EPDS Sunshield | Aluminum | Chromic acid anodized | Leading edge, D8 | Dull luster from AO exposure |
| D4 EPDS Sunshield | Aluminum | Chromic acid anodized | Trailing edge, D4 | Reddish brown contamination film |
| D8 Mod VI Panel | Aluminum | Chromic acid anodized | Leading edge, D8 | Dull luster from AO exposure |
| D4 Mod VI Panel | Aluminum | Chromic acid anodized | Trailing edge, D4 | Reddish brown contamination film |
| D8 SCU Cover | Aluminum | S13GLO | Leading edge, D8 | Crazed rough surface |
| D4 SCU Cover | Aluminum | S13GLO | Trailing edge, D4 | UV degraded; Darkened |

The D8 EPDS sunshield was an aluminum panel 42 by 93 cm having a thickness of 0.1 cm (40 mil), and was painted with a white thermal control paint (Chemglaze A-276) with an underlying primer coat to promote adhesion. The thickness of the paint was approximately 75 microns (3 mil). This paint consists of an inorganic titanium dioxide pigment in an organic polyurethane binder. After the exposure to the space environment, the paint binder at the surface of the paint layer had been eroded away by atomic oxygen, leaving a powdery coating of loose pigment particles. This surface was quite fragile and contained thousands of impact craters varying in size from below 0.001 to 0.093 in. in diameter. The largest crater penetrated through the aluminum. Surrounding most of the craters was an area of delaminated, or spalled paint or an area of roughened texture. The delamination occurred in intermediate layers of paint in which the top layer was folded over the outer edge of the delamination area, leaving a thin layer of paint still adhering to the aluminum substrate. An area of bare metal or melt zone was present between the crater and the delamination area on the larger craters of about 0.005 in. diameter and up. Most of these larger craters had raised rims surrounding the crater cavity, and, in some cases, patches of red or brown primer paint could be seen around the craters or on top of the raised rims. Most of the smallest craters were not visible through the 10X eyepiece, but the impacts were detected by the presence of the delamination zones, which were much larger in diameter than the actual crater by a factor of about 25. Delamination zones of 0.001 in. were observable. Figure V-1 shows photos of representative impacts in this sunshield.

About 2400 impacts were recorded with damage zones of 0.001 in. (25 micron) or greater in an area of the panel measuring 15 by 42 cm. Subsequently, the remainder of the panel was surveyed by counting only those craters with diameters of 0.001 in. or greater. A total of 701 impacts were counted, which corresponds to 1795 impacts/m$^2$ for craters 0.001 in. or greater. Most of the craters were circular; however, 26 of these were oblong, possibly indicating that the impacting particles were highly oblique. The delaminated paint surrounding many of the craters was lifted in large flakes just above the aluminum substrate surface. Some craters appeared dark inside, possibly because they were deeper or contained residue, and, in some cases, a dark spot could be seen inside the crater. This may also be due to lighting artifacts. The largest impact was a 0.090 in. diameter hole through the aluminum panel with a 0.21 in. melt zone and a delamination area of about 1 in. In general, this panel was unique due to the absence of paint binder at the surface and revealed evidence of very small impacts, which were not detectable on other LDEF surfaces or samples.

## B. D4 EPDS Sunshield

The EPDS Sunshield located on tray D4 was identical to the D8 sunshield prior to launch. Measurements of the paint of this surface indicated a thickness of about 60 microns (2.3 mils), a slightly thinner coating than the D8 sunshield. However, after exposure to the space environment, the Chemglaze A-276 paint darkened severely due to UV radiation.[2] Since the trailing edge of LDEF saw little atomic oxygen, there was no erosion of the paint's polyurethane binder. Thus, the surface of the sunshield consisted of a dark-brown glossy painted substrate. The response of this surface to debris/micrometeoroid impact was, therefore, quite different from the D8 sunshield. A total of 72 craters with diameters of 0.001 in. or greater was counted on the 43 by 93 cm panel, which translates to 184 craters/m$^2$. The largest crater was 0.020 in. in diameter. Although in many cases there was an area of bare metal around the crater, presumably due to melt, there was no area of delamination beyond the melt zone. In some cases, a loose flap of paint was still suspended over the area of bare metal surrounding the crater. Seven of the craters were oblong, indicating highly oblique impact. Some black spots were observed inside many of the craters and were possibly due to a primer coat. Brown primer residue was also observed around many of the crater
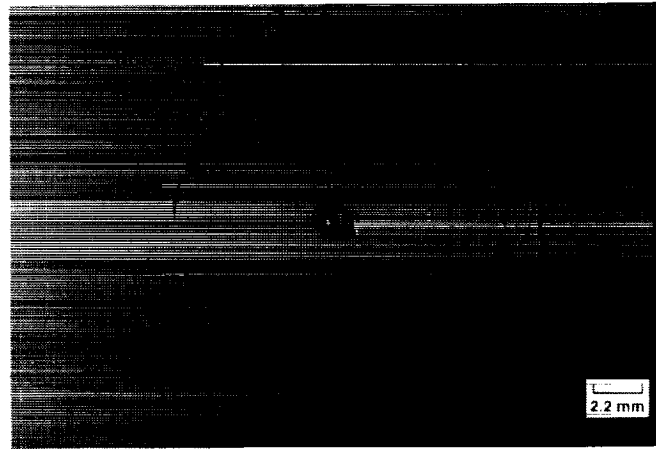
368

(a)

(b)

(c)

(d)
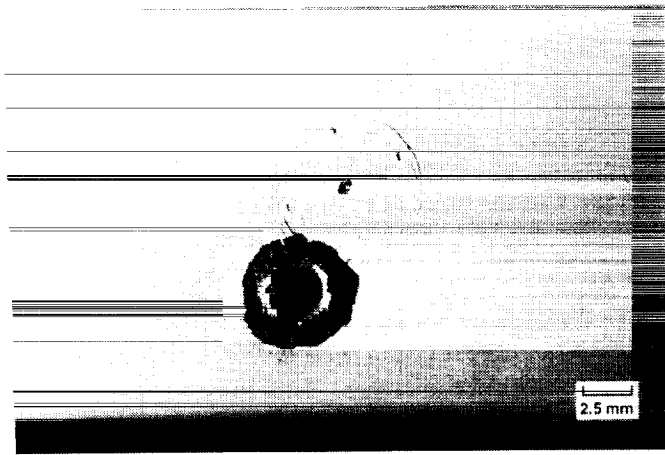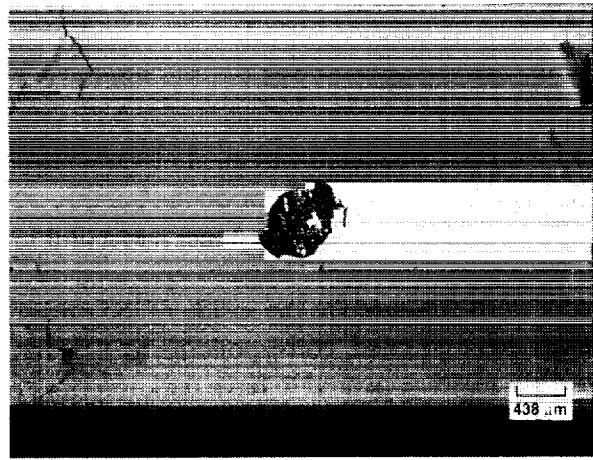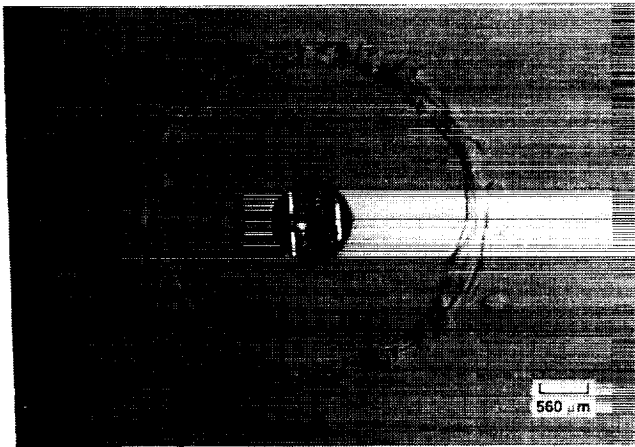
**LANDSCAPE**

Figure V-1. Representative impacts in the D8 EPDS sunshield.

369

rims. In addition to craters, there were many circular areas of various sizes with a yellowish-green stain. Figure V-2 illustrates representative craters from this panel.
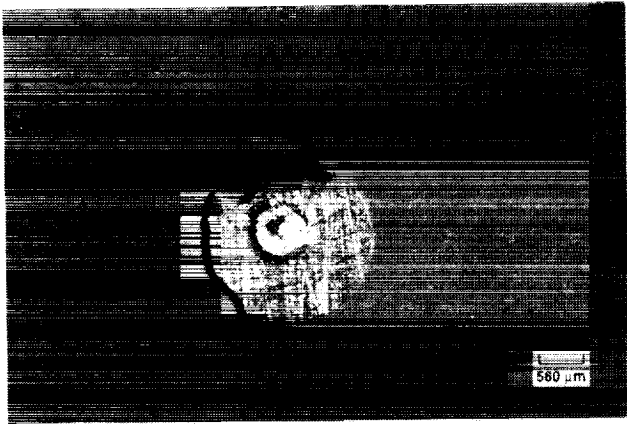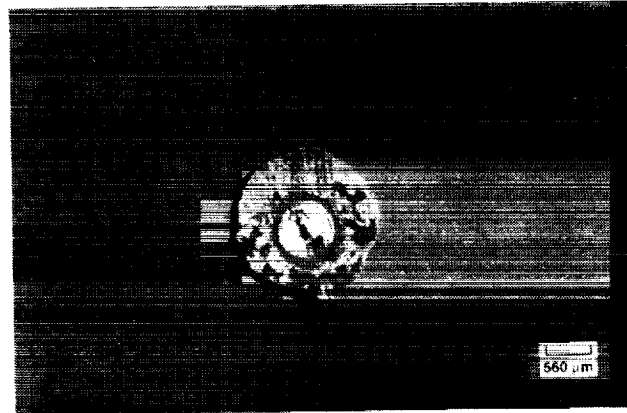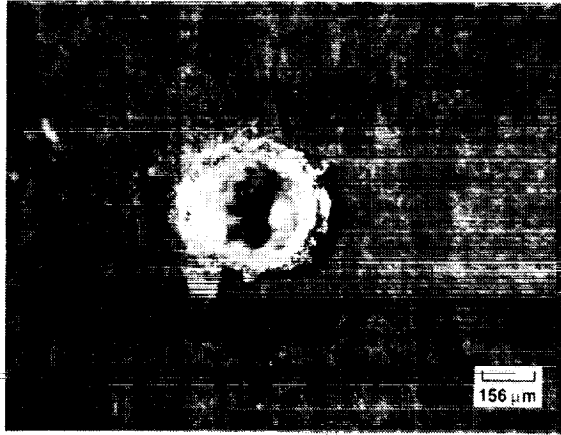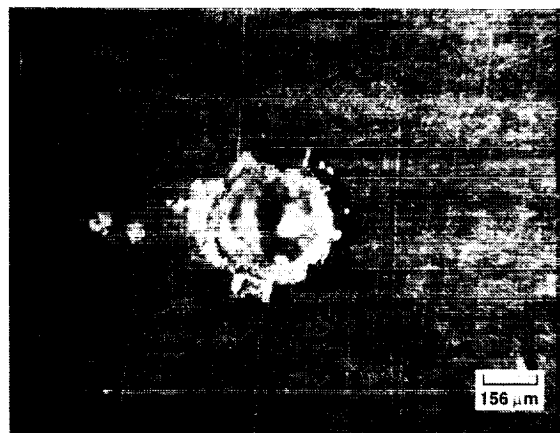

## C. D8 EECC Sunshield


The D8 EECC sunshield was an aluminum sheet 0.16 cm (63 mil) thick measuring 41 by 45 cm mounted over the vacuum canister on the D8 tray. The surface was chromic acid anodized for thermal control purposes. After retrieval, the panel had a dull luster, presumably due to interaction with the leading edge atomic oxygen environment. Impacts appeared as craters with raised walls of aluminum. The diameters of the craters were measured to the inside of the raised walls. A total of 316 craters with diameters of 0.001 in. and greater were counted, corresponding to 1713 craters/m². The largest crater was 0.039 in. diameter. Some of the craters appeared to have dark interiors or dark spots within the crater. This may be due to lighting artifacts. Several oblong cavities were also observed, but these had no raised walls and were presumed to be flaws or gouges in the aluminum surface. Figure V-3 depicts typical damage due to impacts on this panel.


## D. D4 EECC Sunshield


The D4 EECC sunshield was identical to that on D8 prior to launch; however, after LDEF retrieval, the surface of the aluminum panel was still shiny but had a reddish tinge due to staining from the ubiquitous contamination on LDEF.[2] There were also circular areas of brown residue of various sizes. The panel had the same flaws as the D8 sunshield. A count of 58 craters of 0.001 in. diameter and greater was made, or 314 craters/m². The largest crater was 0.015 in. in diameter. The phenomenology of the impacts on this surface was identical to that observed for the D8 panel. Figure V-4 shows representative impacts seen on this panel.


## E. D8 Mod VI Panel

The D8 Module VI panel was a small companion panel to the D8 EECC sunshield panel mounted adjacent to it on the edge of the canister drawer. In construction, it was identical to the EECC sunshields, except it was smaller, measuring 14.1 by 37.5 cm. The appearance of the material after retrieval was similar to the D8 EECC sunshield as previously described. This panel had 134 craters larger than 0.001 in., and the largest measured 0.020 in. in diameter. The crater density for this panel is then 2534 craters/m². Impacts in this surface were identical to those seen on the D8 EECC sunshields, which are shown in Figure V-3.

(a)

(b)

(c)

(d)
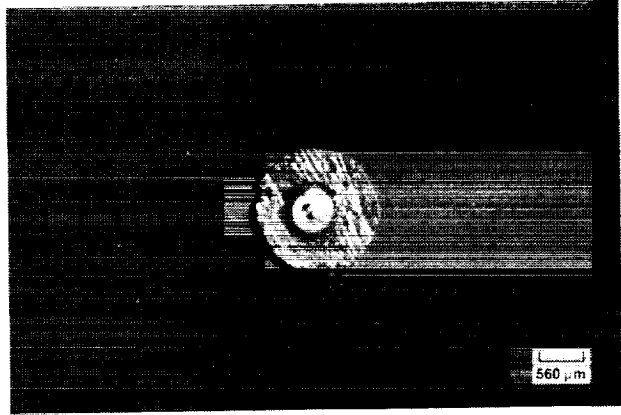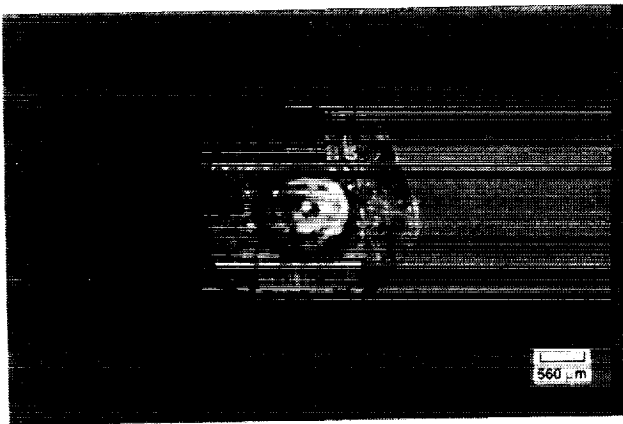
LANDSCAPE

Figure V-2. Representative impacts in the D4 EPDS sunshield.

(a)

(b)

(c)

(d)
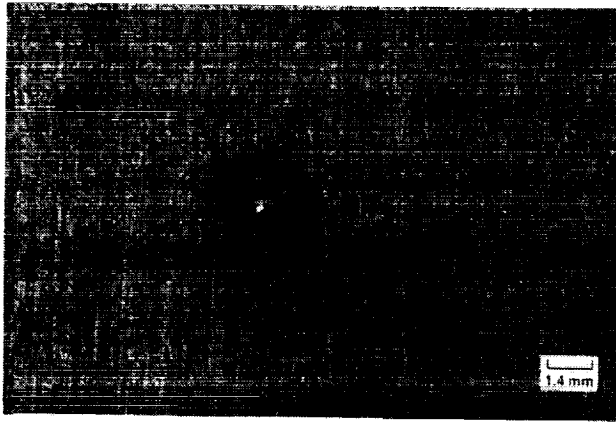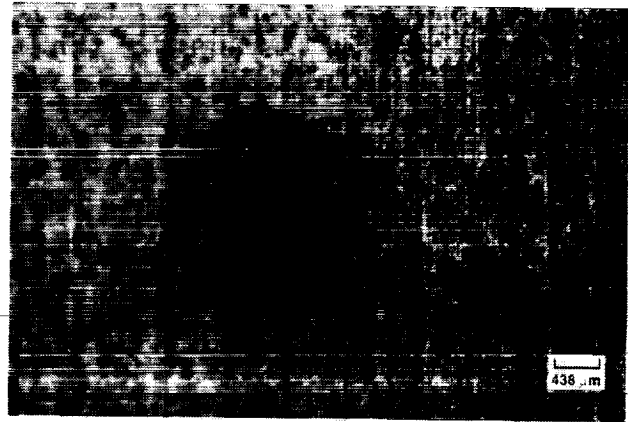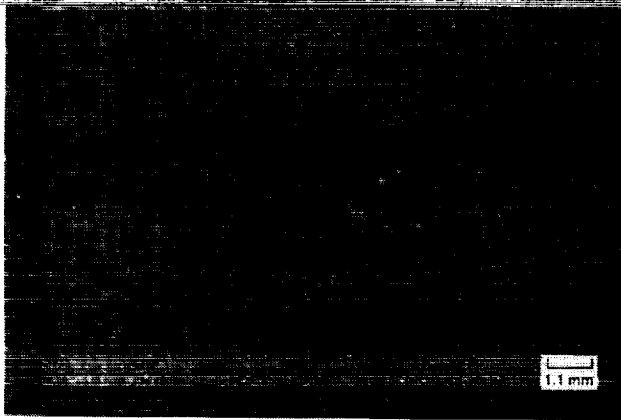
**LANDSCAPE**

Figure V-3. Representative impacts in the D8 EECC sunshield.

(a)            (b)

(c)            (d)
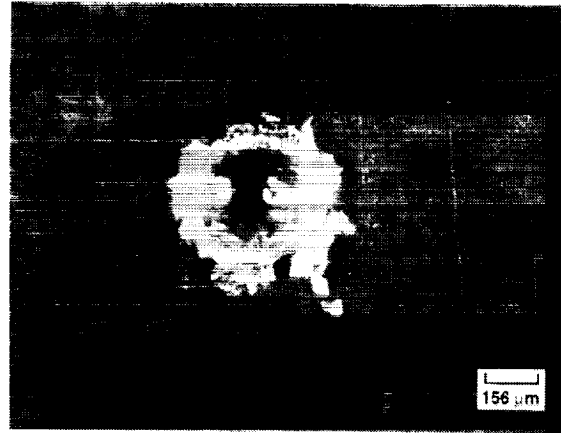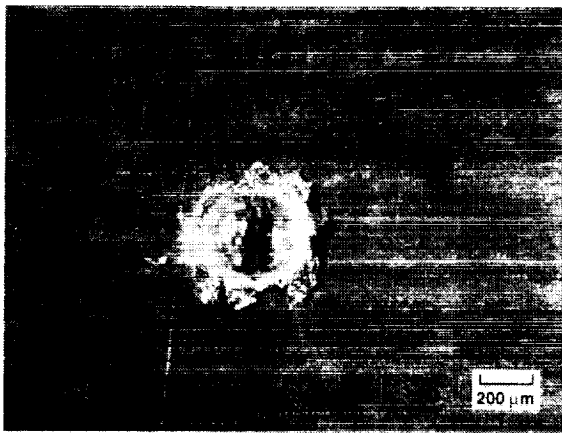
**LANDSCAPE**

Figure V-4. Representative impacts in the D4 EECC sunshield.

## F. D4 Mod VI panel

As with the panel previously described, this was a companion anodized aluminum panel that shielded the edge of the drawer of the EECC on the D4 tray. The appearance of this panel after LDEF recovery was similar to the D4 EECC cover in that it was shiny and had a thin contaminant film. Examination of this panel indicated 19 craters over 0.001 in. in diameter, the largest being 0.015 in. The crater density is 359 craters/$m^2$. As above, impacts in this surface were identical to those observed in the D4 EECC sunshields.

## G. D8 SCU Cover

The D8 SCU cover was a box sunshield that fit over the signal conditioning unit on the D8 tray. It was constructed of aluminum sheet 0.086 cm (34 mils) thick and was double walled on the top surface, the surface scanned in this study. The aluminum was painted with a white thermal control paint, S13GLO, which is a zinc oxide pigment based paint that uses potassium silicate to encapsulate the pigment for UV stability. The binder for this paint is a methyl silicone material similar to GE RTV 602. The thickness of the paint was 230 microns (9 mils). This paint has significantly different mechanical properties than the Chemglaze A-276 paint used for the EPDS sunshields, primarily due to the elastomeric silicone binder, which imparts flexibility. The paint on the retrieved D8 SCU cover was crazed; however, it was still somewhat flexible and resilient, and the binder was still intact even after exposure to atomic oxygen. However, surface analysis using XPS indicated that a silicon dioxide coating had formed from the exposure. Moreover, the cover generally retained its white color in spite of the exposure to UV radiation. This was due to the interaction of atomic oxygen with the damaged material. The mechanism of this whitening process is still under investigation. The texture of the surface was quite rough as originally applied to the surface; the surface resembled, more than anything else, a stucco wall. This caused some difficulty in seeing and counting small impacts. In this material, the delaminated areas around the impacts were not folded back as on the D8 EPDS sunshield, but were simply eroded areas tapering down towards the craters. Bare metal between the crater and the delaminated area was observed on only three craters of the 59 that were counted in the diameter range of 0.001 in. and up giving a crater density of 434 craters/$m^2$. The largest crater was 0.075 in. in diameter with a 0.4 in. diameter area of bare metal surrounding the crater, with no apparent delamination of the paint beyond this melt zone. This impact would have punctured the aluminum if the surface had not been double thickness. The impact produced a deep crater in the material with a depth of 1.8 mm. This surface gave a lower crater density count than the other D8 panels, probably because the smaller impacts left no trace on the textured and resilient paint surface. Figure V-5 illustrates the response of this material to impacts.

374

(a)



(b)
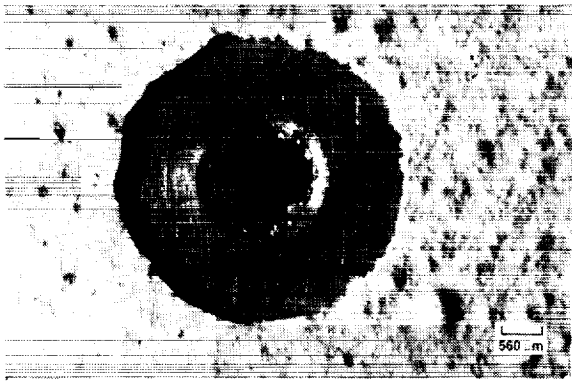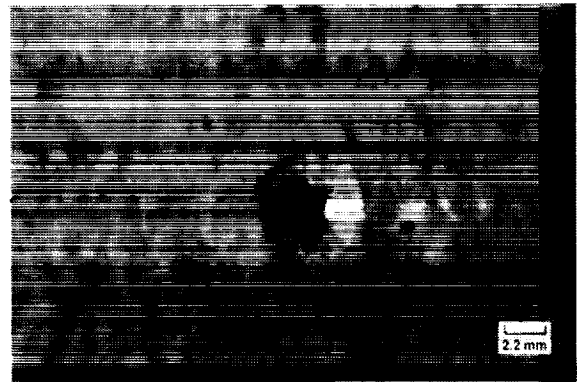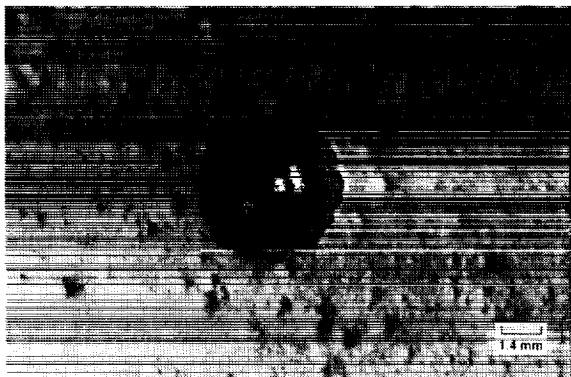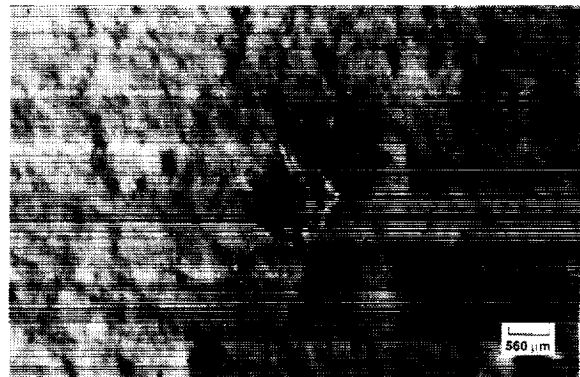


(c) **LANDSCAPE** (d)



Figure V-5. Representative impacts in the D8 SCU cover

## H. D4 SCU Cover

The D4 SCU Cover was identical to the D8 cover prior to launch. The thickness of the base aluminum and the paint were essentially identical to the D8 SCU cover. However, exposure to the space environment produced a darkening of the paint due to UV radiation. Since this cover saw little or no atomic oxygen, there was no observed cleanup of the surface like that seen on the D8 cover. The surface was covered with a network of hairline cracks. Each crater also had hairline cracks spreading radially from the rim and extending for about 0.05 to 0.2 in. beyond. The cracks were easily observable because of their lighter color relative to the paint surface. A low count of 15 craters 0.001 in. in diameter and larger gave a crater density of 108 craters/m$^2$. The largest crater was 0.010 in. in diameter. Interesting photos of this surface are presented in Figure V-6.

## I. Summary

The raw counts for these various surfaces are presented in Table III, including the normalization to craters/m$^2$. Table IV gives the ratio of leading edge (D8) to trailing edge (D4) impacts for the surfaces.

Table III. Summary of Counts by Surface.

| Surface | Area, cm$^2$ | Raw Count | Counts/m$^2$ |
|---|---|---|---|
| D8 EPDS Sunshield | 3906 | 701 | 1795 |
| D4 EPDS Sunshield | 3906 | 72 | 184 |
| D8 EECC Sunshield | 1845 | 316 | 1713 |
| D4 EECC Sunshield | 1845 | 58 | 314 |
| D8 Mod VI Panel | 528.8 | 134 | 2534 |
| D4 Mod VI Panel | 528.8 | 19 | 359 |
| D8 SCU Cover | 1357.9 | 59 | 434 |
| D4 SCU Cover | 1394.9 | 15 | 108 |

Table IV. D8/D4 Impact Ratios for Various Surfaces.

| Surface | D8 Impacts/m$^2$ | D4 Impacts/m$^2$ | Ratio D8/D4 |
|---|---|---|---|
| EPDS Sunshields | 1795 | 184 | 9.76 |
| EECC Sunshields | 1713 | 314 | 5.46 |
| Mod VI Panels | 2534 | 359 | 7.06 |
| SCU Covers | 434 | 108 | 4.02 |

(a)



(b)



(c)

**LANDSCAPE**



(d)
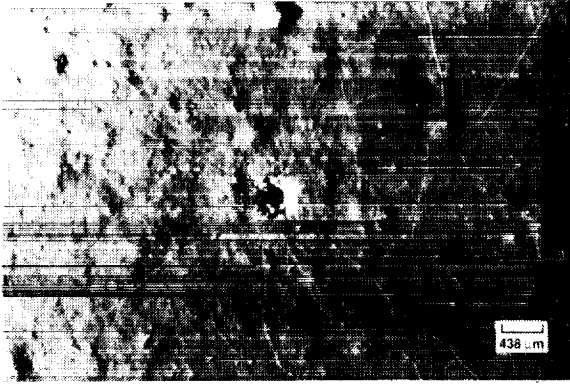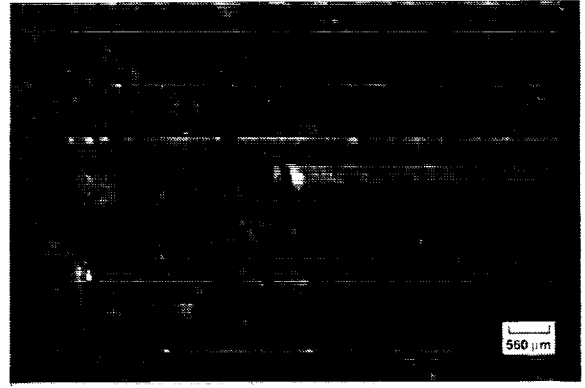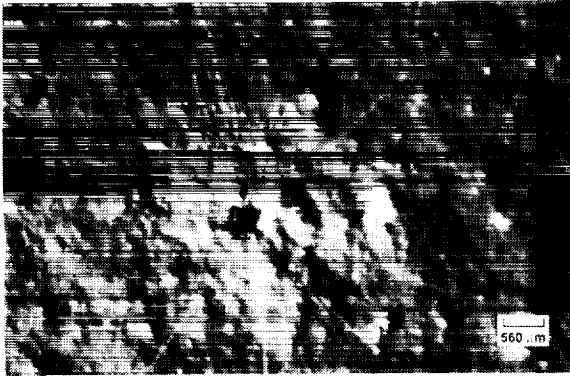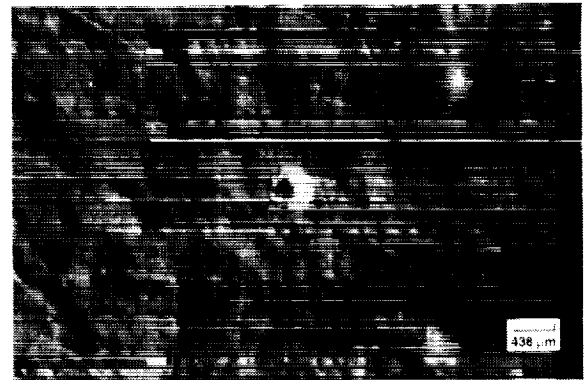
Figure V-6. Representative impacts in the D4 SCU cover

This data is presented in the following graphs, which are of two types: dot plot and histograms. A plot of each type is included for each surface studied. To illustrate the size differences between the various surfaces, the dot plots have been scaled to actual relative sizes. The histograms have been plotted with both linear and logarithmic ordinates. This information is presented in Figures V-7 through V-15. It will be seen from these plots that the distributions are different for each surface. This might be expected statistically, and may have to do with the different material response of the different surfaces and/or surface roughnesses. The ratio of leading edge to trailing edge (D8/D4) impact craters in any particular size range can be discerned from these plots. This, too, is not very constant and varies from about 1:1 to 10:1.

Before comparing this data to a model, a statistical analysis of the data was performed to determine the effect of the different panel surface areas on the sampling accuracy. This becomes especially important for the larger craters where the number of impacts per area is very small. Since the positions of all craters were determined in the survey, it was easy to compute distances between various craters to determine the mean distances between impacts. The spatial distribution of 701 craters with diameters greater than 0.0025 cm (25 microns) on the D8 EPDS sunshield was examined mathematically for areas of localized crater clusters. This involved calculating the mean crater separation distance and the standard deviation of the mean. Groupings of clusters would tend to decrease the mean crater separation and increase the relative standard deviation of the mean compared to a random spatial distribution. Using these statistics, comparisons of the D8 EPDS sunshield to computer-generated, random and clustered models indicated a definite "random" character to the actual crater distribution. This suggests that over time a net random spatial distribution of craters would be expected on a ram facing LEO-exposed surface. Results on the D4 EPDS sunshield were also found to be consistent with a "random" spatial distribution; however, lower crater densities on the trailing edge created a larger statistical uncertainty.

# D8 EPDS Sunshield (Crater Locations)



Legend:
- · 0.001" to 0.003"
- ∘ 0.004" to 0.010"
- O greater than 0.010"
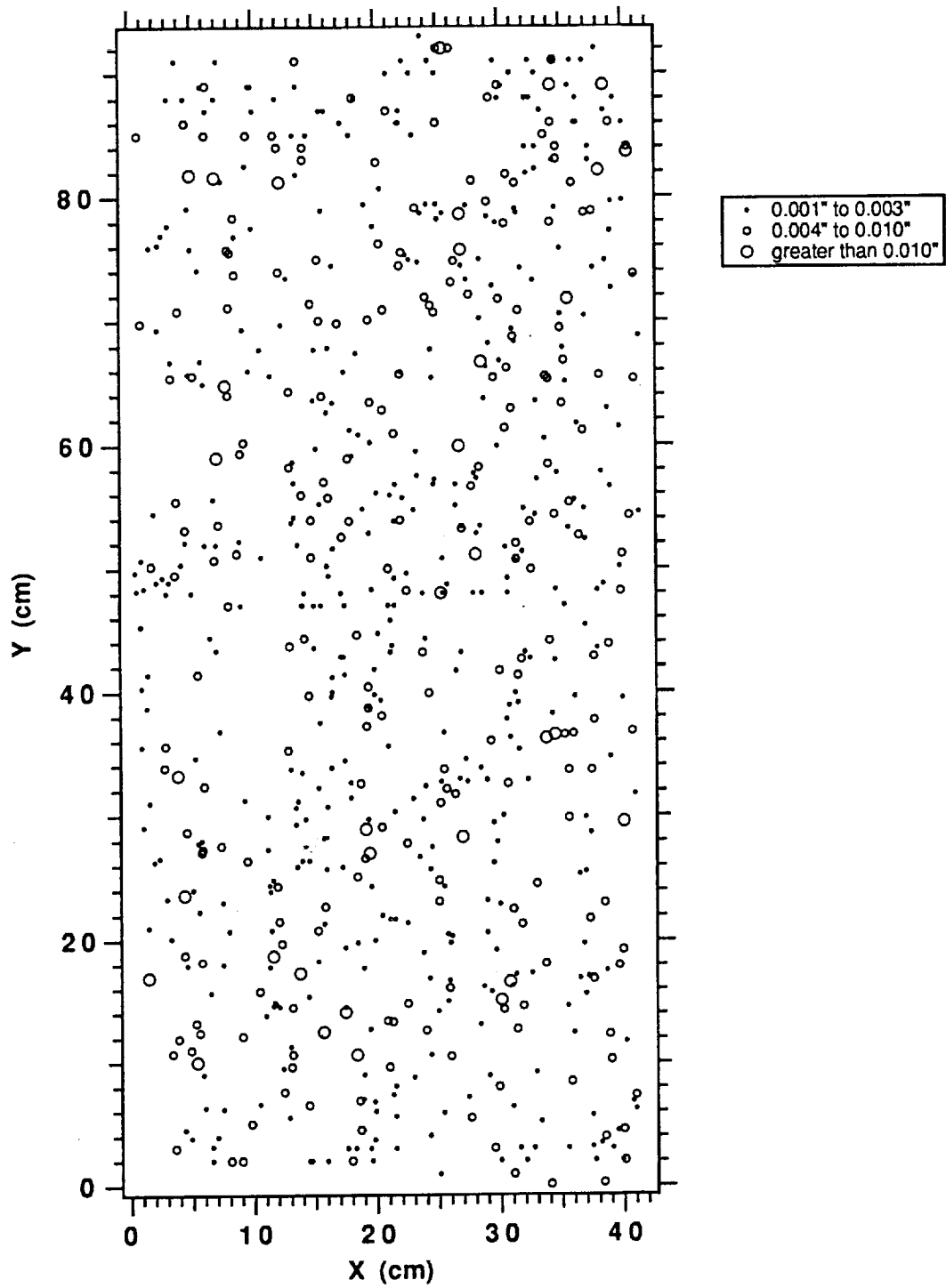
Figure V-7. Dot plot for D8 EPDS sunshield.

379

**D4 EPDS Sunshield (Crater Locations)**
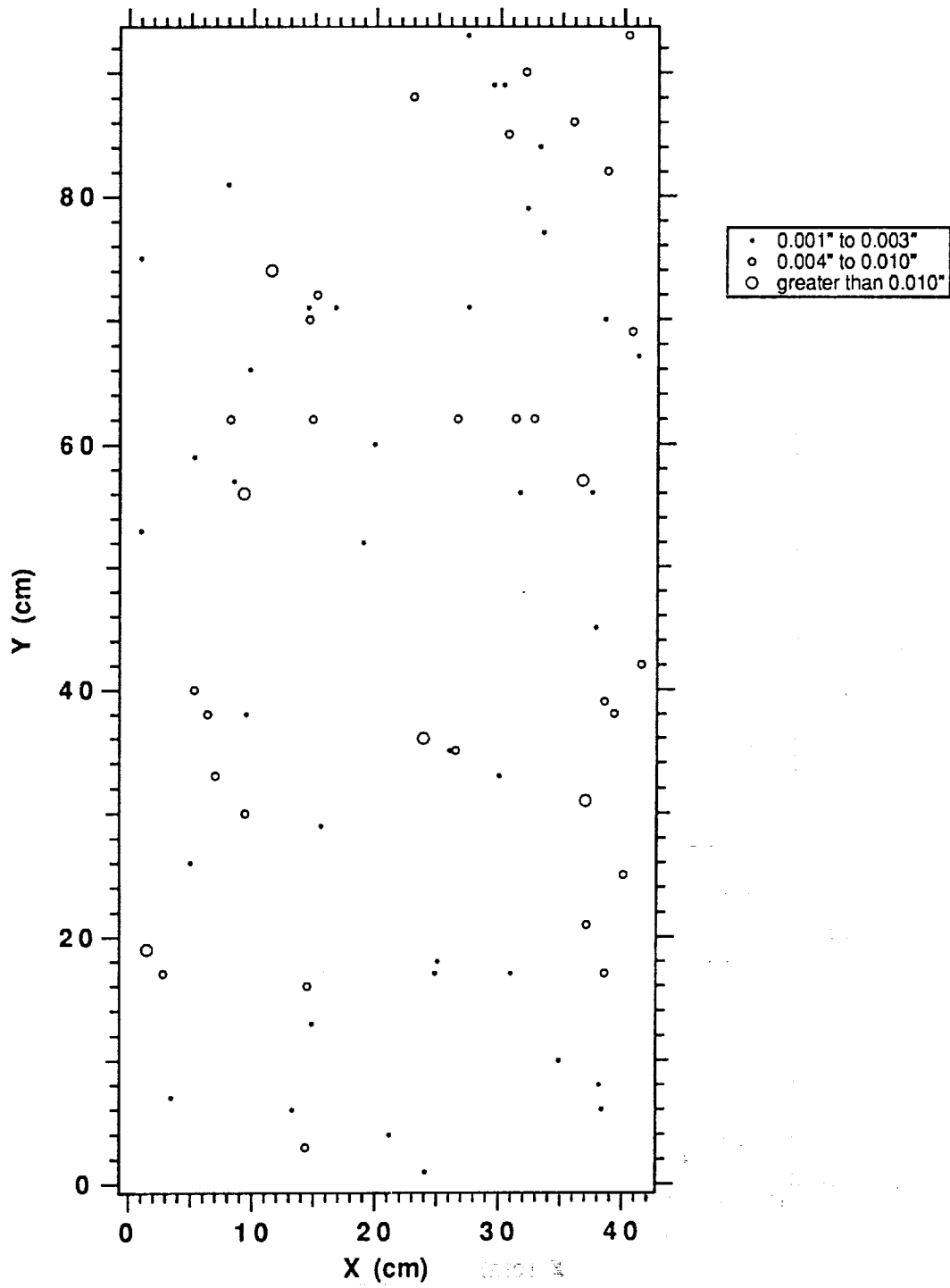
Figure V-8. Dot plot for D4 EPDS sunshield.

380

**D8 EECC Sunshield (Crater Locations)**

**D4 EECC Sunshield (Crater Locations)**



| | |
|---|---|
| · | 0.001" to 0.003" |
| o | 0.004" to 0.010" |
| O | greater than 0.010" |
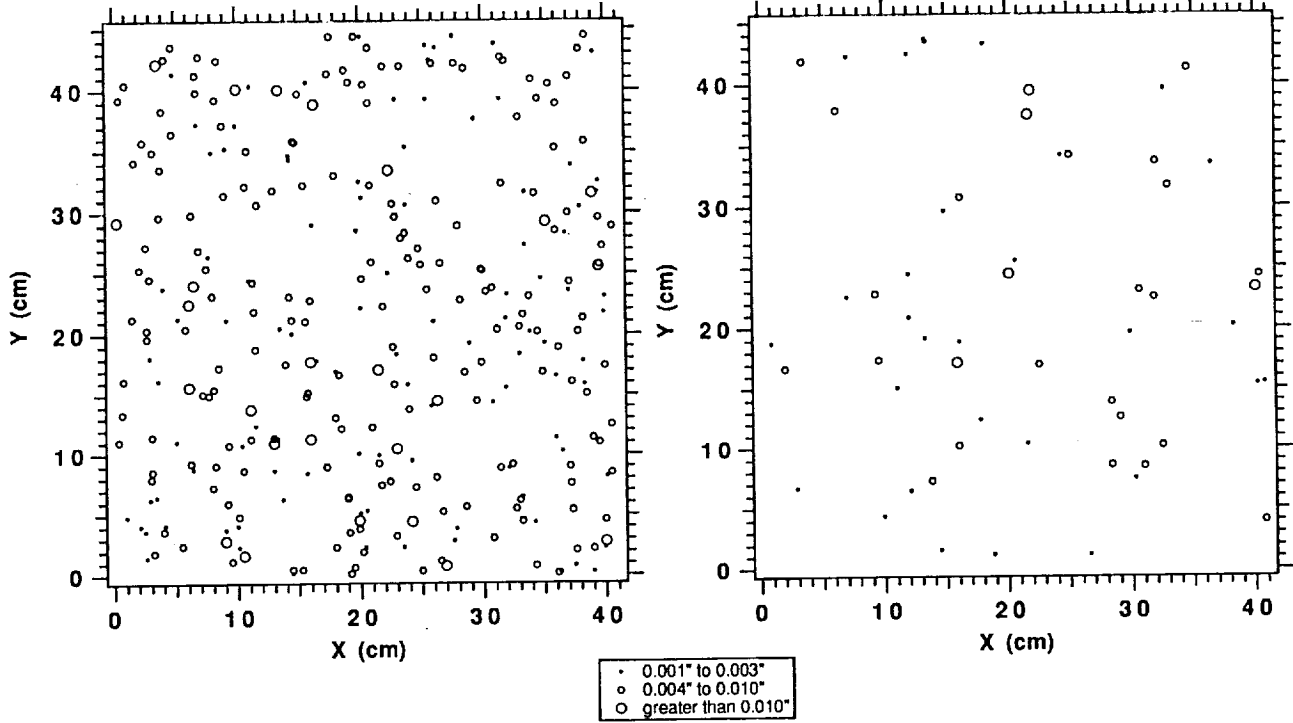
**LANDSCAPE**

Figure V-9 Dot plot for D8 and D4 EECC sunshields

**D8 Module VI Panel (Crater Locations)**
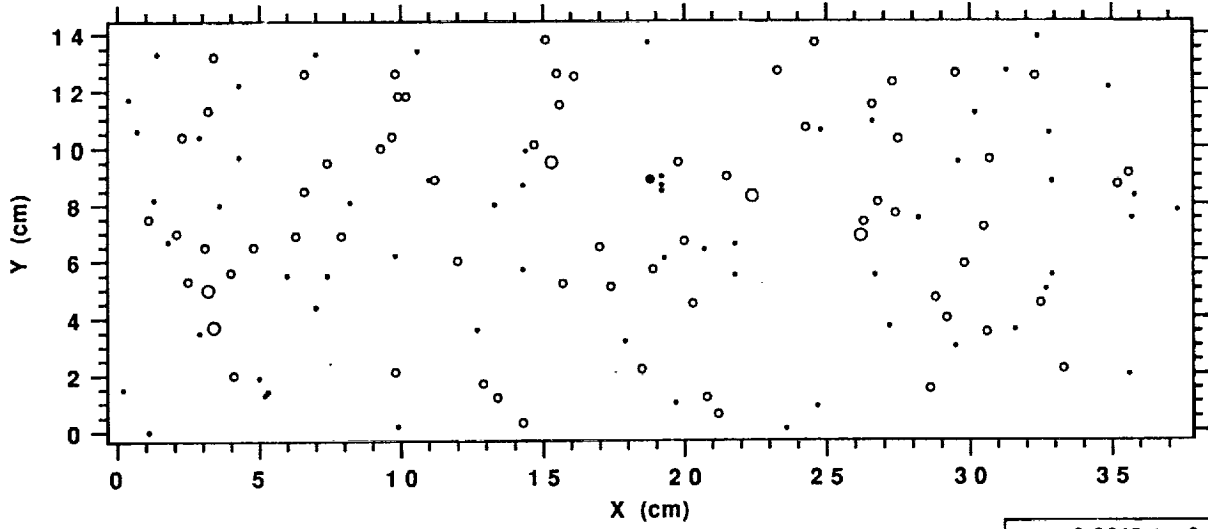
Y (cm)

X (cm)

| | |
|---|---|
| • | 0.001" to 0.003" |
| ○ | 0.004" to 0.010" |
| ○ | greater than 0.010" |

**D4 Module VI Panel (Crater Locations)**

Y (cm)

X (cm)
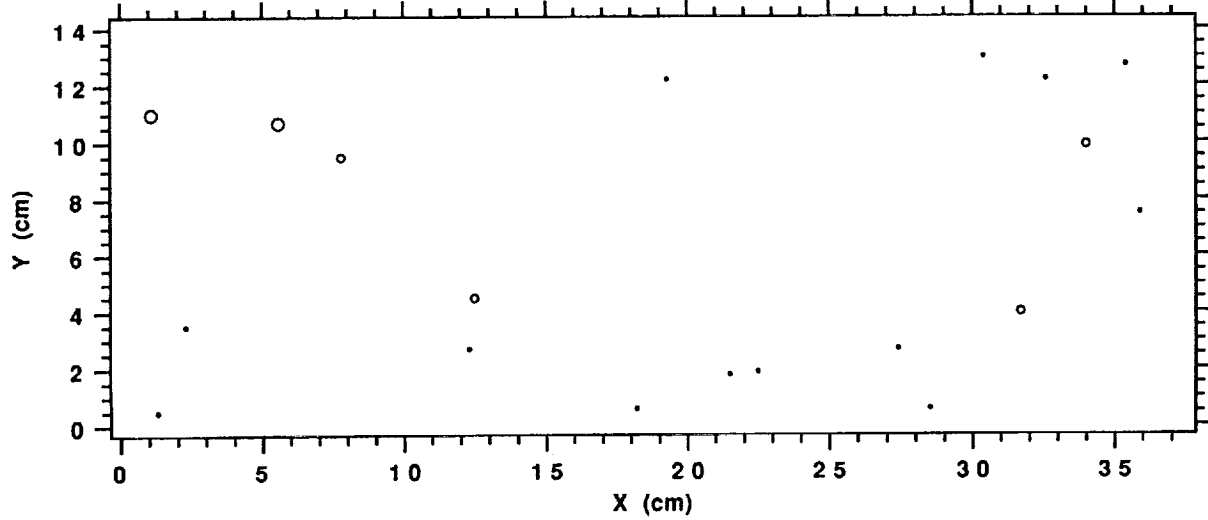
**LANDSCAPE**

Figure V-10 Dot plot for D8 and D4 Mod VI panels

382

**D8 SCU Cover (Crater Locations)**     **D4 SCU Cover (Crater Locations)**

| | |
|---|---|
| 0.001" to 0.003" |
| 0.004" to 0.010" |
| greater than 0.010" |
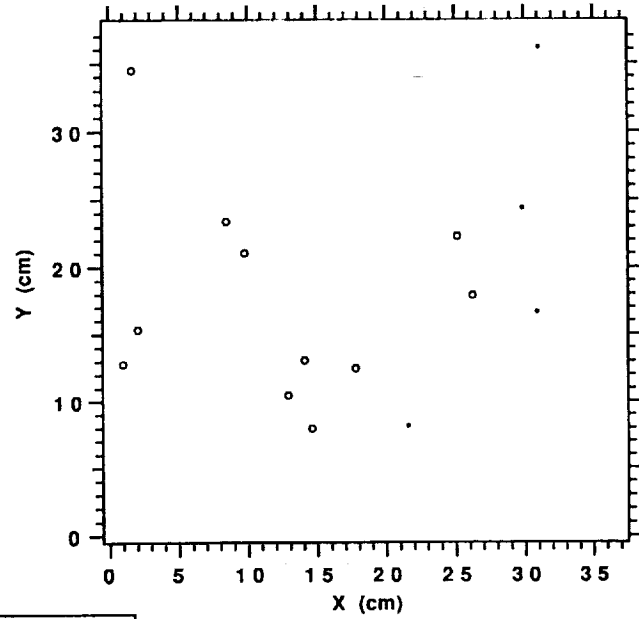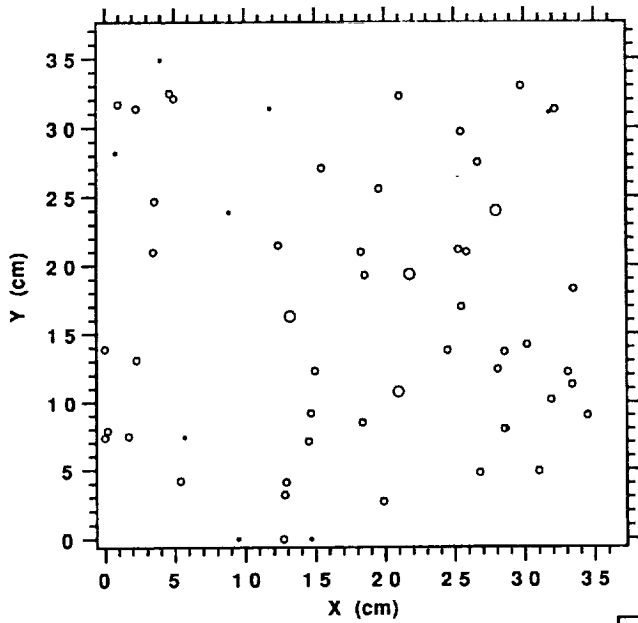
## LANDSCAPE

Figure V-11  Dot plot for D8 and D4  SCU covers.

**EPDS Sunshields**
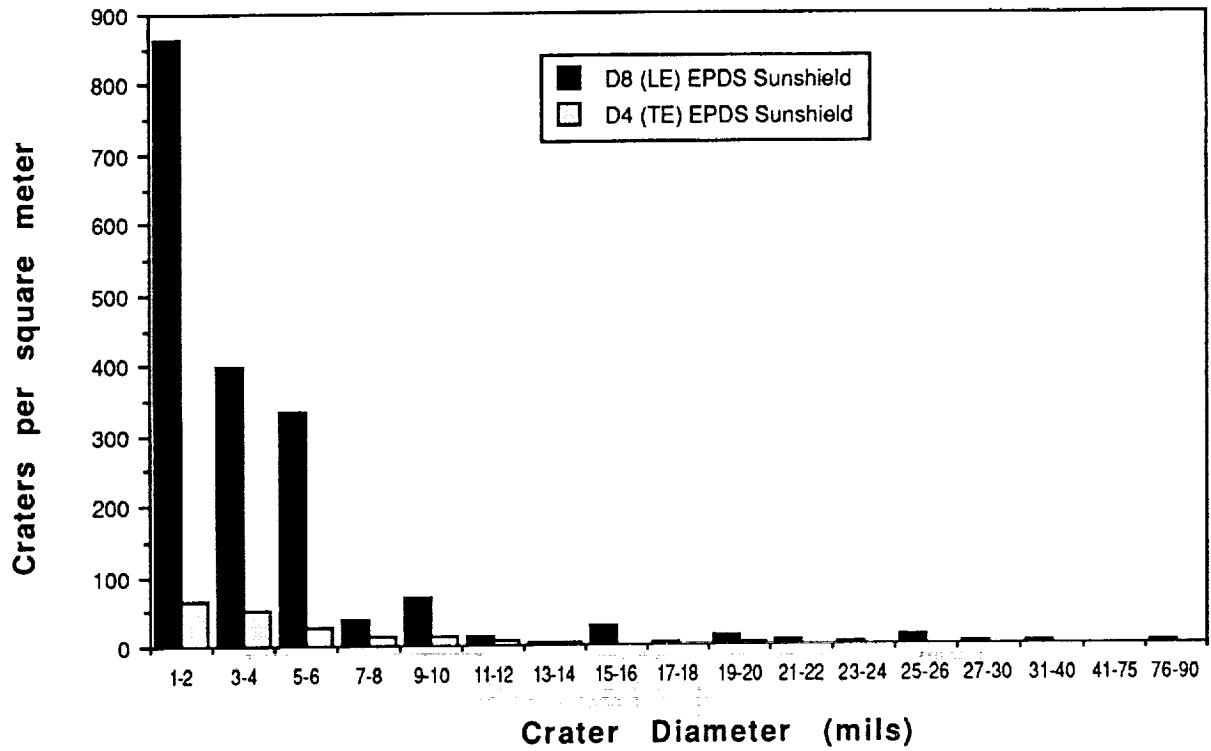


**SCU Covers**
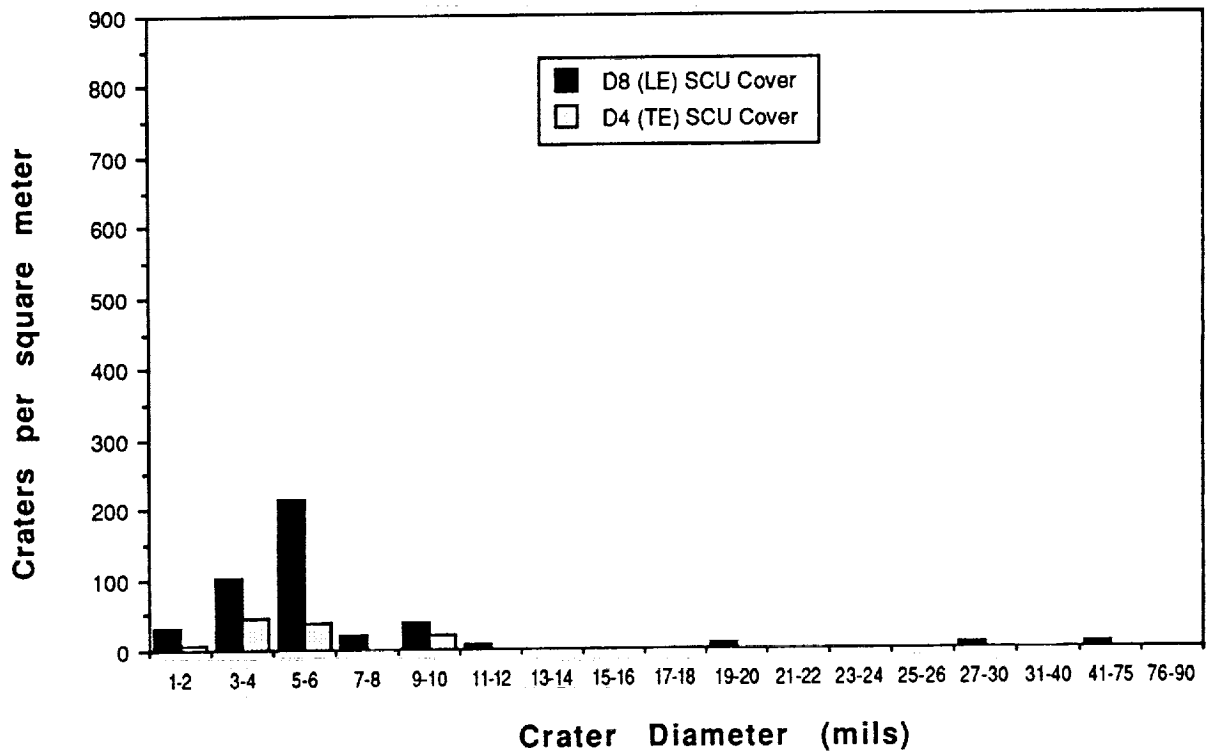


Figure V-12 Linear histograms for painted surfaces.

# EECC Sunshields
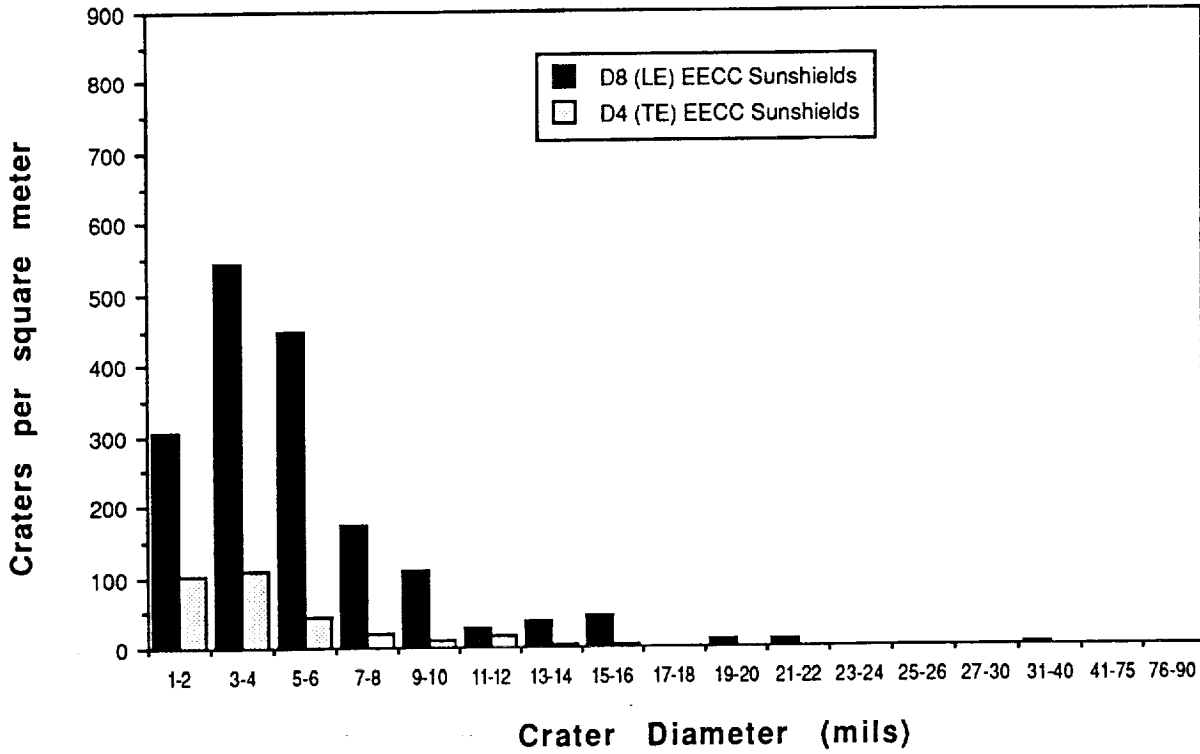


# Module VI Panels
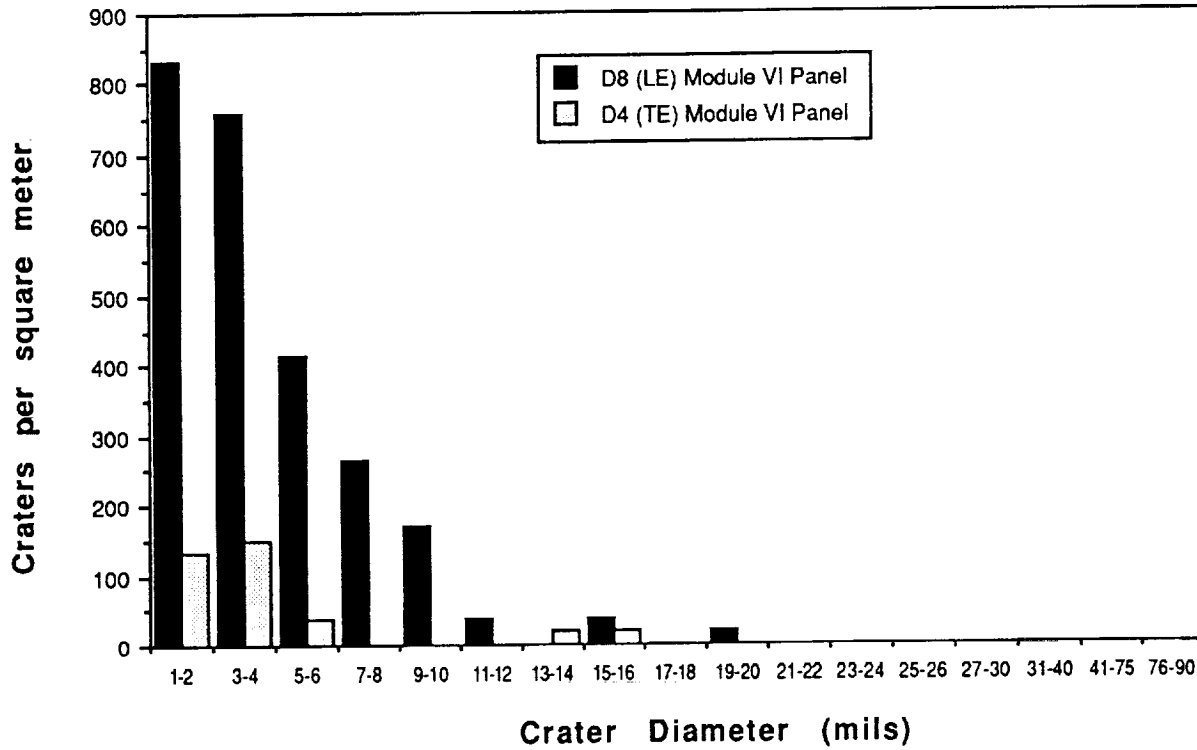


Figure V-13 Linear histograms for anodized surfaces.
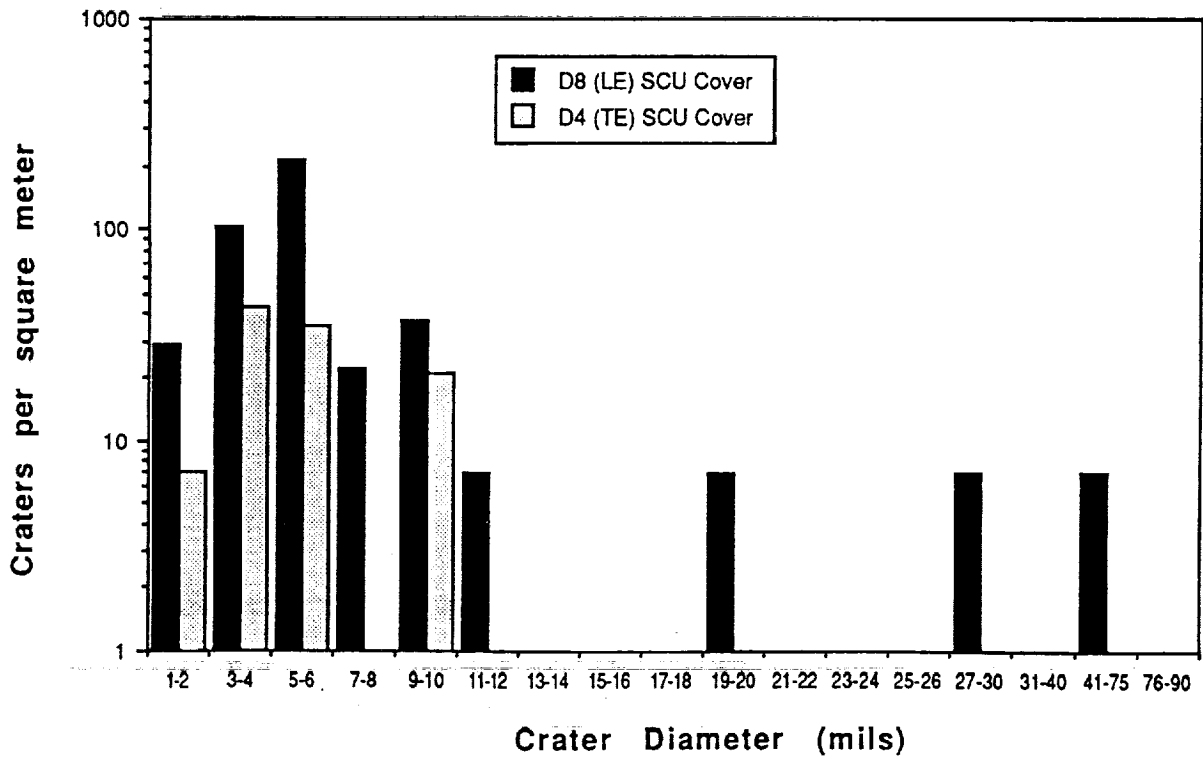
# EPDS Sunshields

Figure V-14 Log histograms for painted surfaces.

## SCU Covers

## EECC Sunshields



Crater Diameter (mils)

## Module VI Panels



Crater Diameter (mils)
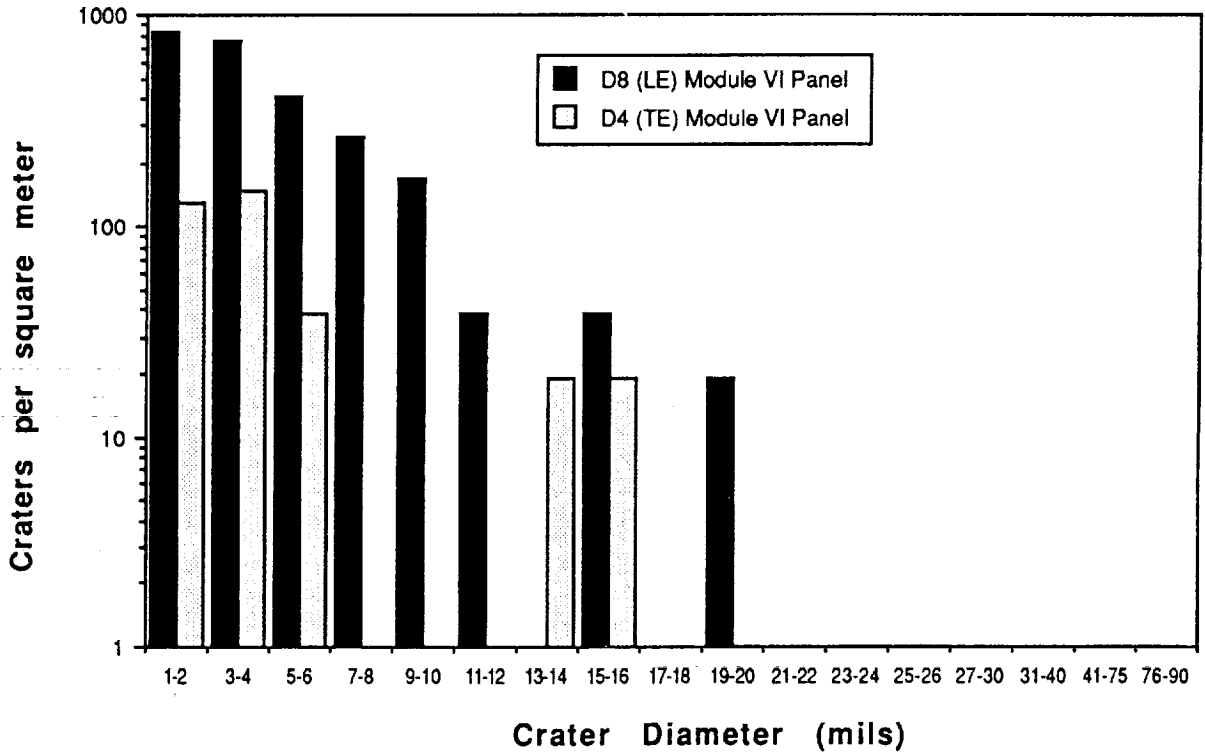
Figure V-15 Log histograms for anodized surfaces.

# VI. RESULTS BY MATERIAL

## A. Material Response to Hypervelocity Impacts

The material categories chosen for this discussion — metals, ceramics, glasses, composites, polymers and paints — parallel the categories used in the M0003 sample observation database.[18]

## B. Metals

The general response of aluminum on LDEF to hypervelocity impacts has already been discussed for the chromic acid anodized aluminum EECC sunshields. Other examples of anodized aluminum and other metals are shown in Figures VI-1 through VI-14.

The response of the black anodized hardware is very similar to the sunshields. Impacts in the hardware are shown in Figure VI-1. In particular, this figure shows SEM photos of the entry and exit sides of a trailing edge (D3) perforation. All of these impacts display the classic raised lip structure, due largely to melt and hydrodynamic flow of the metal. The oxide layer has been shocked away.

Figure VI-2 shows representative impacts in metals. A typical impact crater in a copper mirror is shown in (a). There was no damage to this substrate beyond the area of the impact. In the nickel-coated copper mirror shown in (b), there are spatters of resolidified matter surrounding the craters; however, the damage is similar to that seen in the uncoated copper. While the samples did show some corrosion due to atomic oxygen exposure, this seemed to have no effect on the extent of damage. In (c), a typical crater in bare, polished molybdenum is shown. Only localized damage from the impact was seen in this material. The response of a rhodium foil on aluminum is illustrated in (d). This sample was from the trailing edge of LDEF (Row 3), as opposed to the three previous metals, which were leading-edge specimens. The foil has not been perforated, and there is a large amount of metal flow around the site. It may be that this impact resulted from a slow micrometeoroid.

In contrast to the response of uncoated molybdenum substrates shown in Figure VI-2, the response of coated molybdenum can be quite different. Figure VI-3 graphically depicts the type of damage zone that can occur with hypervelocity impacts in some materials. In (a) we have a thorium fluoride-coated silver mirror on a molybdenum substrate with a 782-$\mu$m crater surrounded by a 1-cm blistered area. It would appear from the shape of the crater and the asymmetric damage zone that this impact occurred at a glancing angle. This type of damage was unusual (blistering without damage to the overlying layers), and its cause is not understood. Remarkably, the thorium fluoride coating was not cracked extensively, and no tarnishing of the silver layer was observed. There were other impacts in this sample, but they did not show the large damage zones observed around this impact. The cause of this difference is not known. It is hoped that further examination of these specimens will reveal more about material response and the effects of such impacts on performance. In (b), there is an impact in molybdenum coated with an aluminum oxide/silicon multilayer coating. Here, the brittle nature of the coating has caused it to crack and delaminate at the impact site. More damage to the sample could be anticipated as the coating flakes off. This sample was in the leading-edge
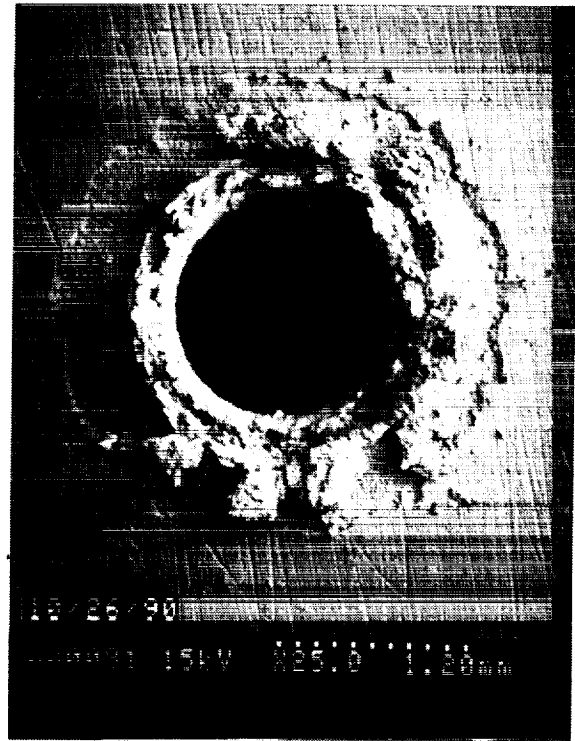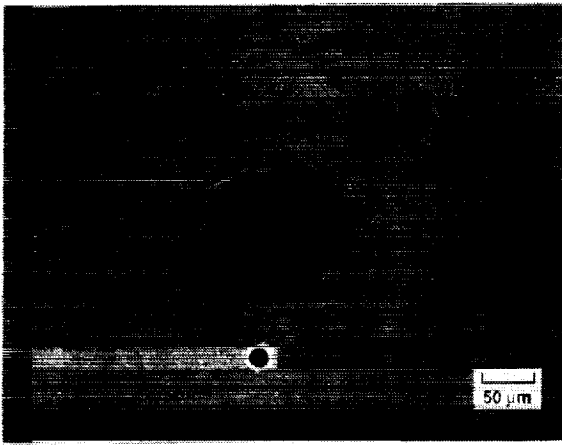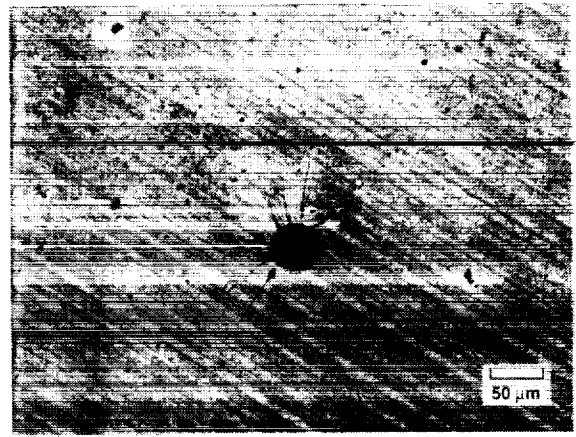
(a)


(b)


(c)
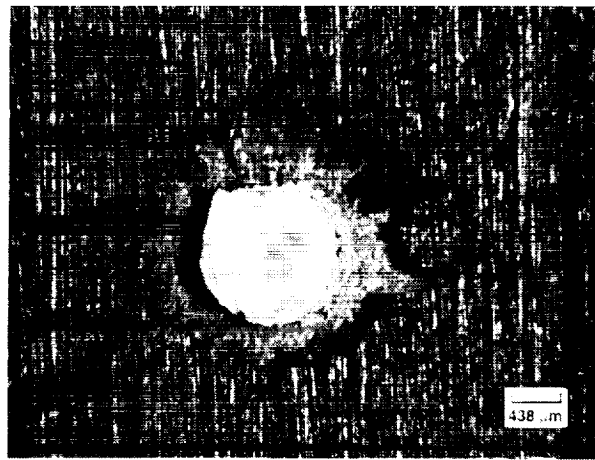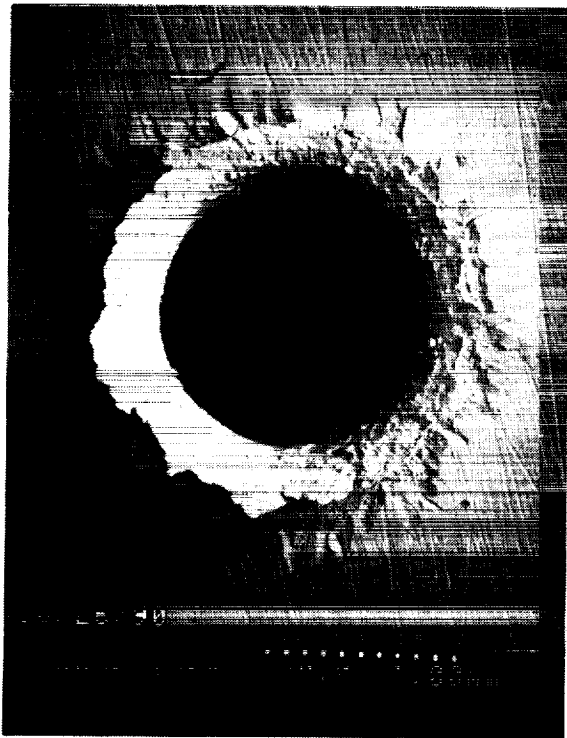
**LANDSCAPE**
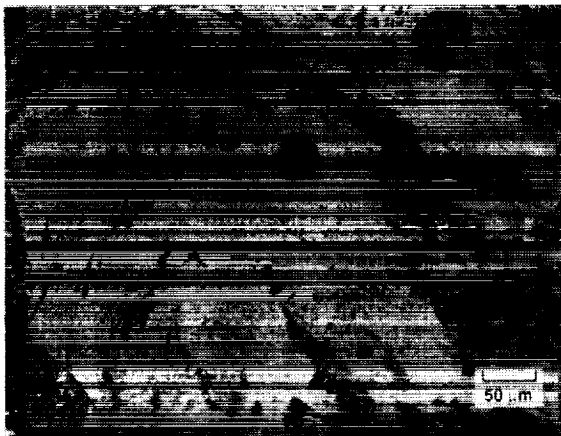

(d)

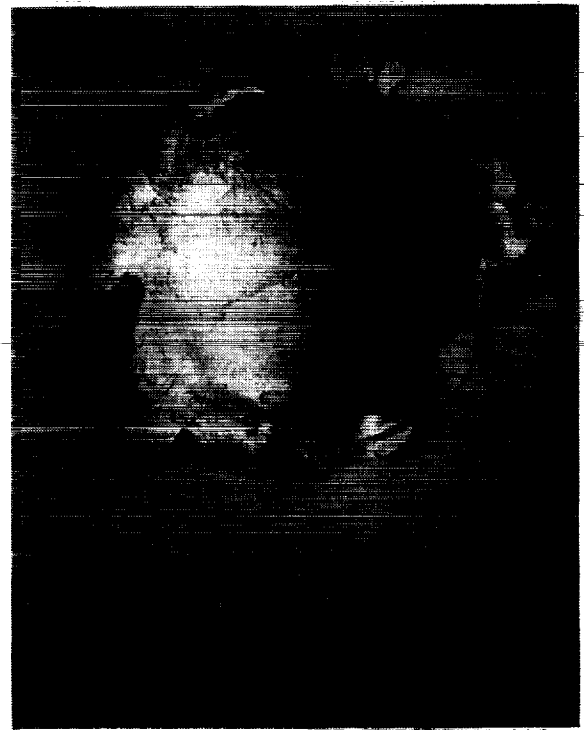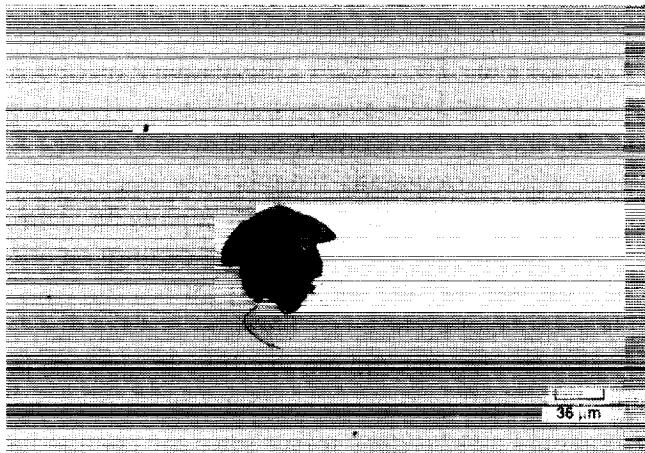Figure VI-1. Typical impacts in the black anodized aluminum MOOO3 hardware.
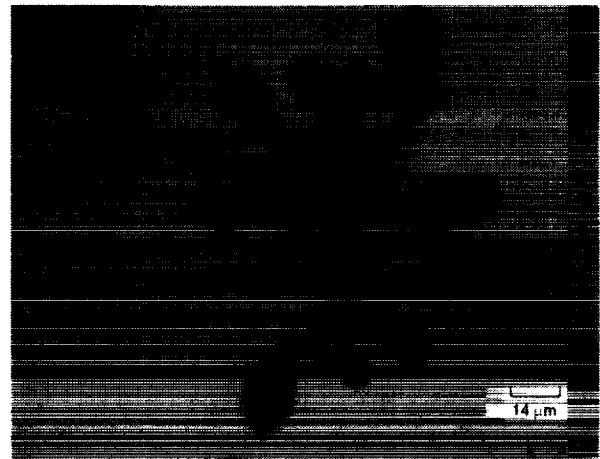
389

(a)

(b)

(c)

LANDSCAPE

(d)

Figure VI-2. Impacts in metals: a) Copper mirror; b) Nickel-coated copper mirror; c) Molybdenum substrate; d) Rhodium foil on aluminum.

(a)



(b)



(c)

Figure VI-3. Impacts in coated molybdenum: (a) Thorium fluoride-coated silver mirror on molybdenum; (b) Alumina/Silicon multilayer coating on molybdenum; (c) ZnS/ThF$_4$ multilayer on molybdenum.

canister, and, therefore, only saw limited exposure to atomic oxygen. An interesting and unusual reaction zone around a ZnS/ThF$_4$ multilayer coating on molybdenum is shown in (c). The cause of this reaction zone is not known, but it is not due to a synergistic effect with atomic oxygen since this sample was mounted in the trailing edge canister.

The response of unmounted molybdenum foils to impacts is shown in Figure VI-4. These are oxide-coated molybdenum foils approximately 2 mil thick. The sample shown in (a) has a SiO2 coating while (b) is coated with a proprietary coating, P-273. The radial cracking of the silica layer is evident in (a); however, no such effect is seen in (b). The exit view shown in (c) indicates considerable spall of the metal. The sample shown in (d) is also oxide coated. The coating has also been shocked away around the impact site.

Figure VI-5 illustrates an interesting impact in a piece of tray hardware, the D8 canister aperture plate; the impactor hit the anodized and Teflon-coated aluminum at an oblique angle, producing a large amount of aluminum spatter on the adjacent sample, a zinc selenide IR witness plate. The aluminum spatter on this sample is shown in (b) and (c). These photos clearly illustrate the type and amount of collateral damage that may occur from hypervelocity impacts, especially to optics.

## C. Ceramics and Glasses

Figure VI-6 illustrates the response of uncoated 7940 fused silica to hypervelocity impacts. In most cases, the damage is localized; however, radial cracking does occur to a limited extent. Contrary to expectations, the cracks did not propagate a great distance from the impact site. The effect of this damage on optical performance and its long-term effects are largely unknown. Coated fused silica as seen in Figure VI-7 often displays crazing or cracking of the coating in addition to chonchoidal substrate cracking; however, sometimes unusual and extensive propagation of cracks is observed, while infrequently there is only localized damage. In Figure VI-8, more impacts to coated fused silica are shown. For example, (a) depicts the damage to magnesium fluoride coatings on fused silica, consisting of chonchoidal cracking. The coating on all magnesium fluoride-coated fused silica samples was crazed, regardless of the location on LDEF. The laboratory control was crazed as well, indicating that this effect is not related to the space environment but may be due to aging, and/or to processing conditions. The crazing of the coatings did not result in an increase in damage area around the craters. Large damage sites surround two small impacts in another sample (b) composed of a sodium fluoride coating on fused silica. This is no doubt a synergistic effect since the coating has been damaged by exposure to UV and/or atomic oxygen, and it is this damaged layer that has been lost or removed around the impact site.

The effect of an impact on a silver-coated, fused-silica, second-surface mirror is shown in Figure VI-9 (a). The impactor produced small, localized damage and no delamination of the coating. Solar cell response to impact phenomena is typical of that shown in Figure VI-9 (b), which indicates some delamination at the impact site and chonchoidal cracking of the substrate. This particular impact is in a gallium arsenide cell. The response of bulk gallium arsenide to this type of impact is illustrated in (c). In this brittle material, the craters were typically small hemispheres surrounded by an irregular-shaped spall zone with many small radiating cracks. This type of damage was common to all electronic materials on the experiment of which the gallium arsenide was just one. None of the impactors perforated any of these materials. Figure VI-9 (d) shows an impact that penetrated a glassy carbon structure with a rhodium coating. The structure is webbed,
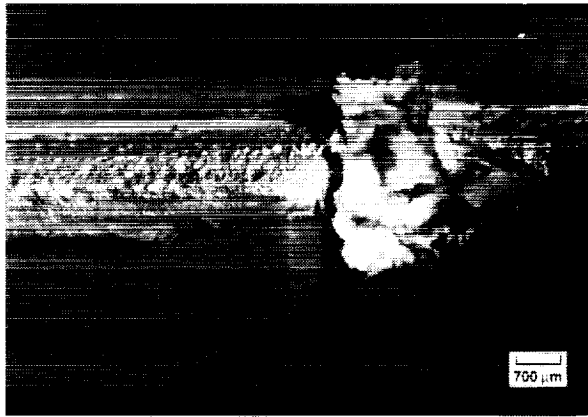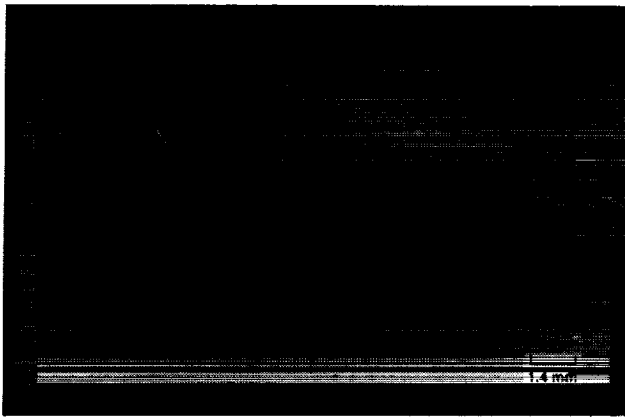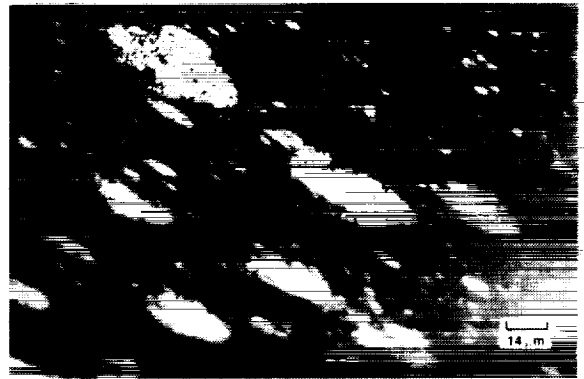
392

(a)

(b)

(c)

(d)
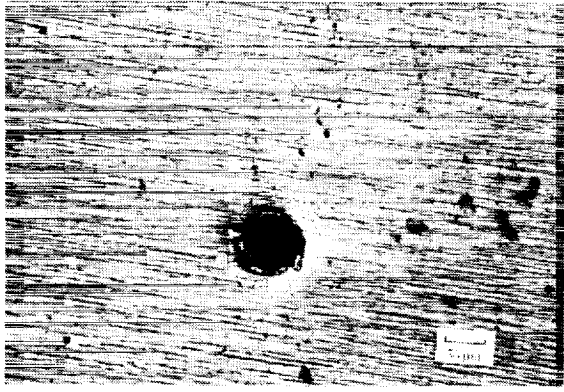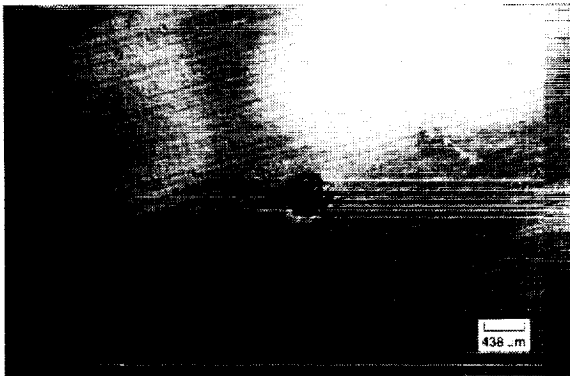
LANDSCAPE

Figure VI-4. Impact perforations in coated molybdenum foils: a) Silica coated; b)
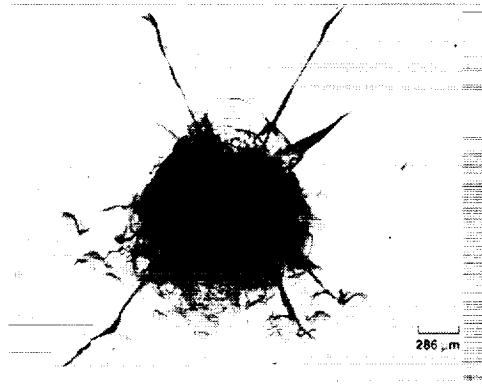P-238 coated; c) exit view of b); d) oxide coated Molybdenum.
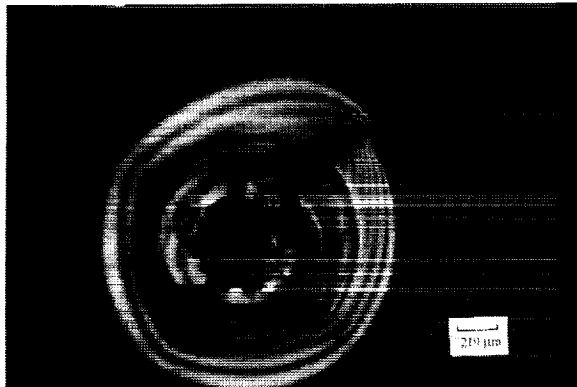
(a)



(b)



(c)

**LANDSCAPE**

Figure VI-5. Impact damage causing collateral damage to optics

(a)



(b)



(c)

**LANDSCAPE**

Figure VI-6. Representative impacts in 7940 fused silica substrates.

(a)

(b)

(c)

(d)
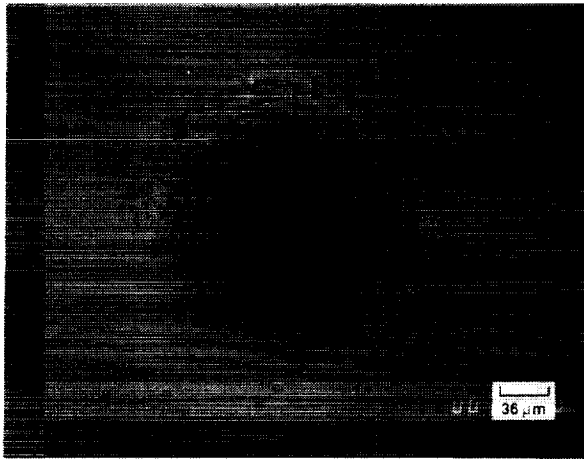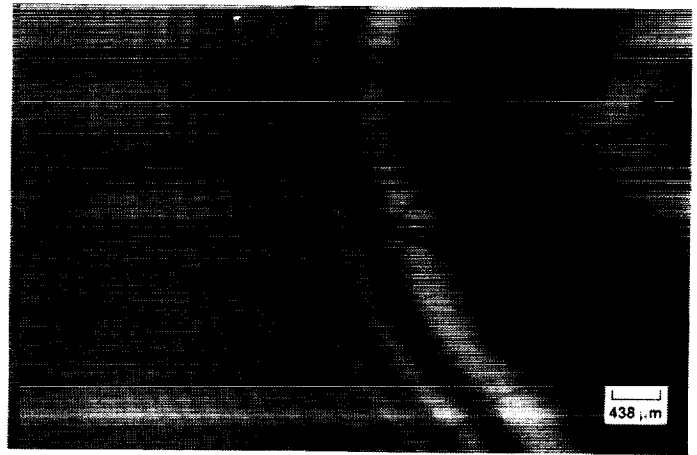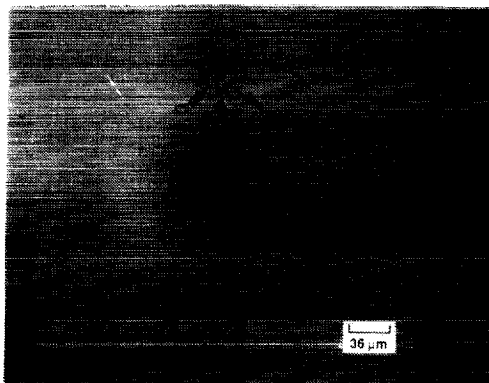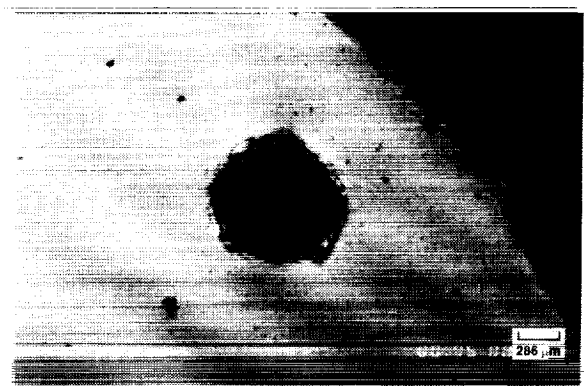
**LANDSCAPE**

Figure VI-7. Response of optical coatings on fused silica to hypervelocity impacts. All coatings are proprietary formulations from Optical Coating Laboratories, Inc.
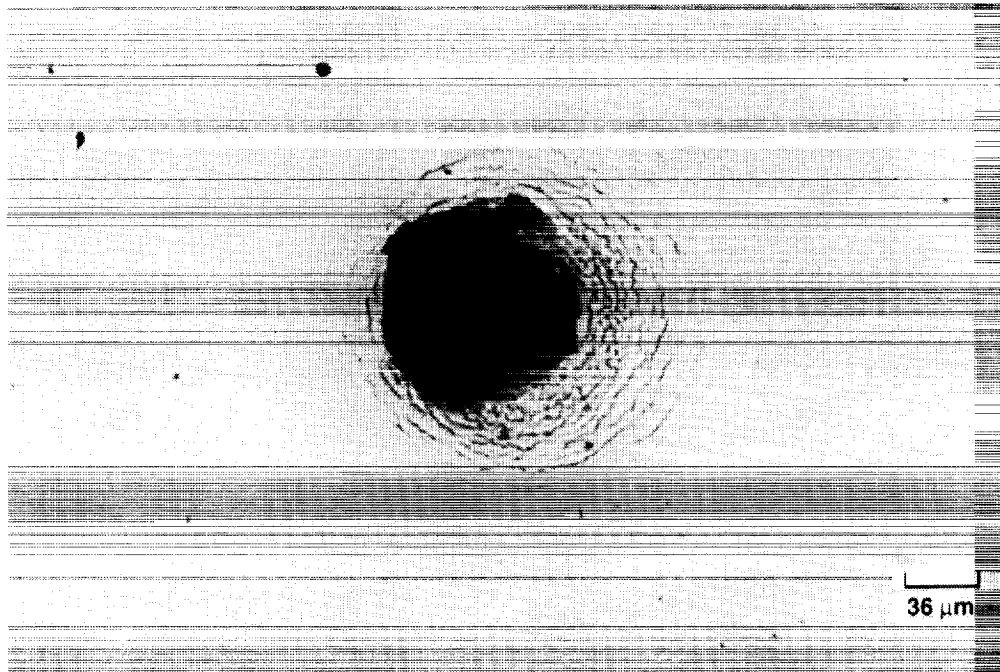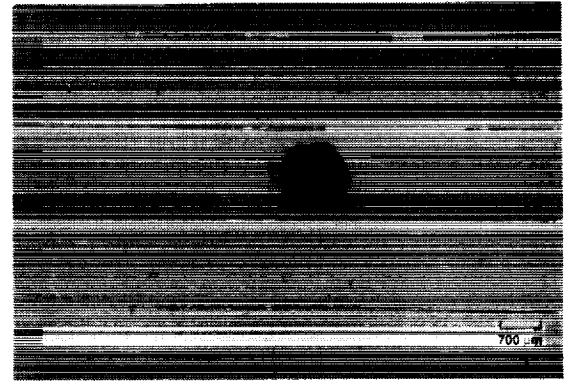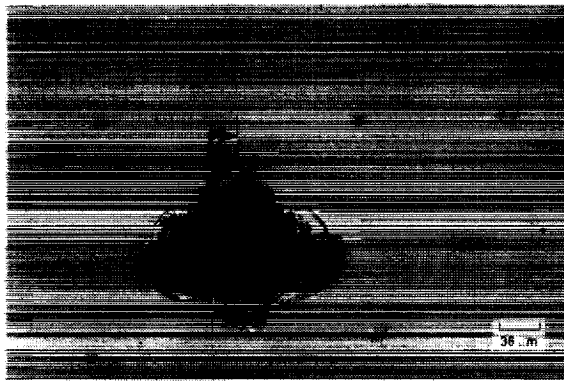
(a)



(b)

**LANDSCAPE**

Figure VI-8. Impact damage to coated fused silica. (a) Magnesium fluoride coating; (b) Sodium fluoride coating.
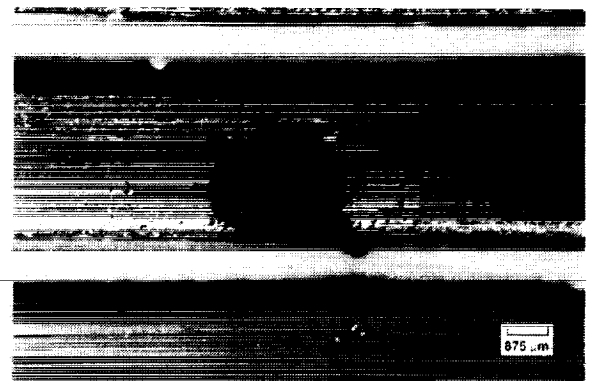
397

(a)

(b)

(c)

(d)
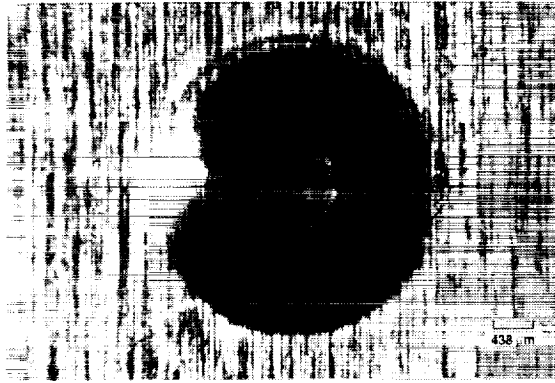
**LANDSCAPE**

Figure VI-9. Impacts in ceramics and glasses. a) OCLI second surface mirror (Silver OSR); b) Gallium arsenide solar cell string; c) bulk Gallium arsenide; d) Rhodium coated glassy carbon.

and significant chonchoidal cracking is evident around the site and under the sidewalls (webbs). The glassy carbon is approximately 2 mm thick at the impact site.
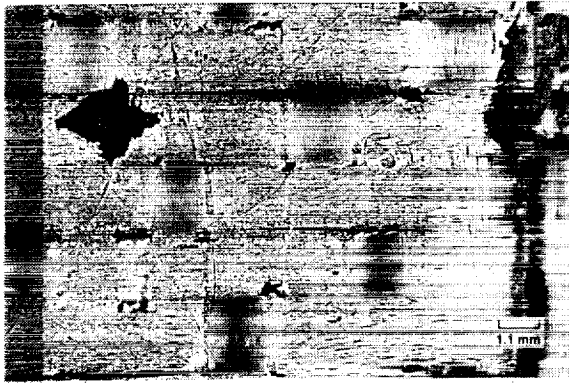
## D. Composite Materials

The response of organic matrix composites, primarily graphite epoxy, to hypervelocity impacts is represented by Figure VI-10. The damage to such materials is generally localized, with some chipping of the matrix in the outer layers of the composite at the crater site. In all cases examined, no perforations were observed. This may be a result of chance or the result of many layers of the composite acting as bumpers to slow down and vaporize the impactor. Metal matrix composites, such as graphite/aluminum, respond differently than the organic matrix composites, and behave much the same as metals to impact phenomenology as shown in Figure VI-11.
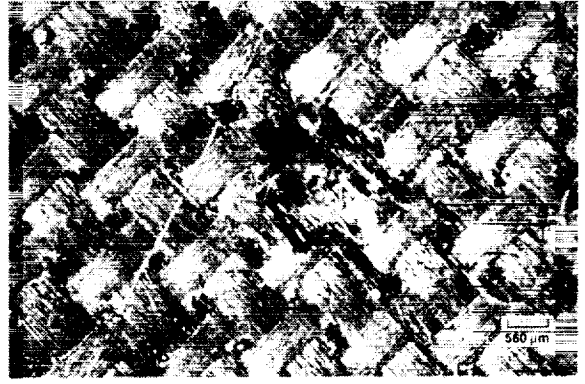
## E. Polymers

Impacts in polymeric materials produced interesting synergistic phenomena primarily due to the exposure of the materials to atomic oxygen on the leading edge and UV on the trailing edge. Figure VI-12 (b) shows the damage around an impact crater in a sample of black RTV 602 located on the trailing edge. The embrittlement caused by UV exposure has produced a large degree of cracking in the material and at the impact site. In comparison, Figure VI-12 (a) shows that an identical sample of this material located on the leading edge displays similar cracking of the material, but, in addition, there is radial, star-type cracking at the impact site due to reaction of atomic oxygen with the surface of the silicone, which produced a glassy surface layer of $SiO_2$. The response of this surface layer to hypervelocity impacts is very similar to that observed with glasses such as silica. The larger degree of radial cracking in this sample relative to bulk fused silica may be due to the greater elastic response of the bulk RTV relative to the outer glassy layer due to the thin nature of this $SiO_2$ layer. Polymeric films that were not metallized did not exhibit unusual impact phenomenolgy or synergistic effects; rather they showed typical circular perforations that are assumed to be only slightly larger than the impactor. An impact site in a Tefzel strip is shown in (c). A plastic-metal laminate that received a perforating hit is shown in (d). This site displays the classic raised lip as a result of the melt and flow of the aluminum and vaporization of the polymer front surface.

Metallized polymer films, however, did indicate some synergistic effects, the most significant being atomic oxygen oxidation of the backside reflective silver layer of silver-teflon. This effect produced a black spot resembling tarnish around the impact site. This is illustrated clearly in Figure VI-13(a). Note also the delamination of the Teflon from the silver layer at the impact site. This was also quite common to this material. Another perforation in (b) shows only small amounts of tarnish at the edges of the crater. Impacts in aluminized Kapton are shown from the backside of the Kapton strip in (c), one being a standard perforation and the other indicating melt and delamination of the aluminum around the impact site. An impact in a front surface aluminized Kapton sample is shown in (d).
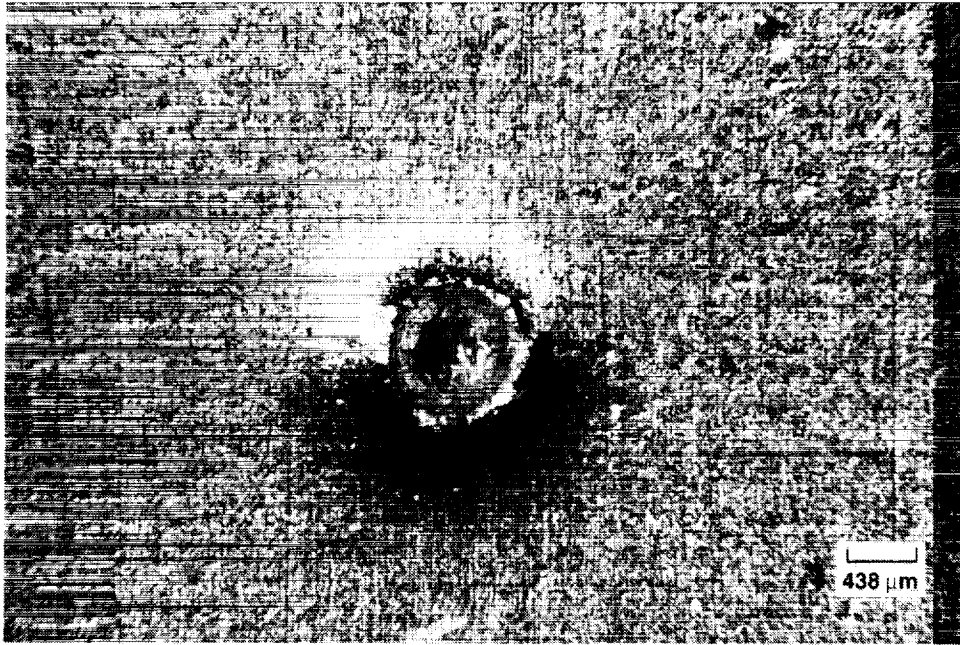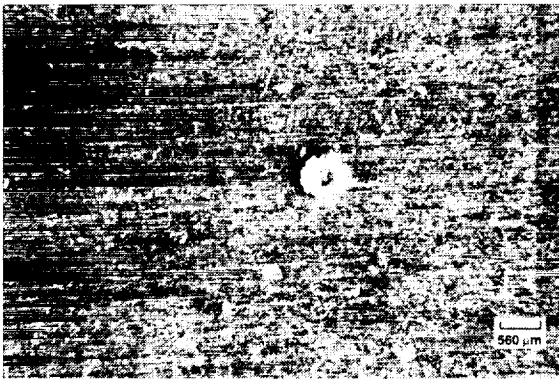
(a)

(b)

(c)

(d)

**LANDSCAPE**

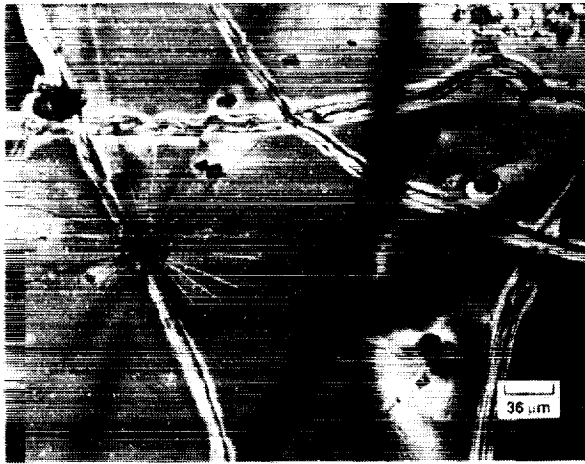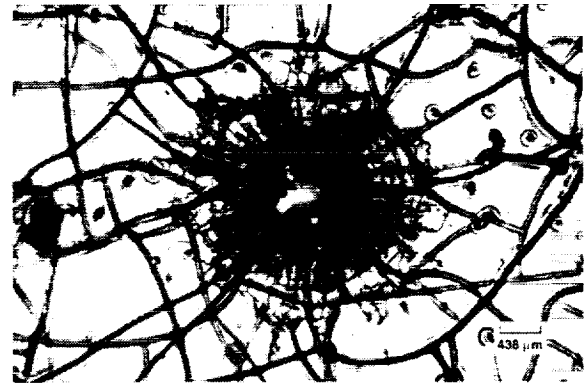Figure VI-10. Representative impacts in organic matrix composites
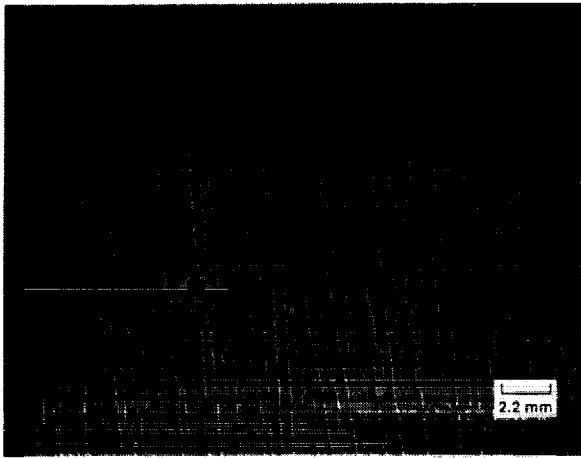
(a)



(b)



(c)

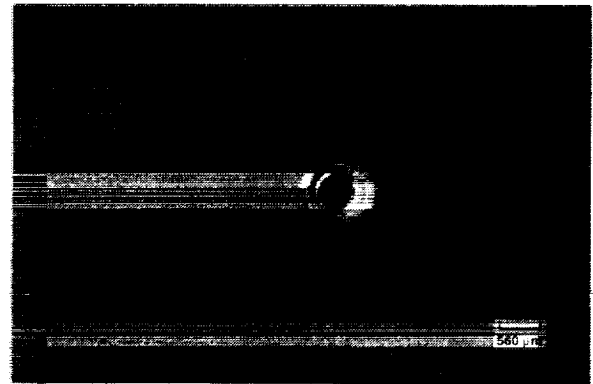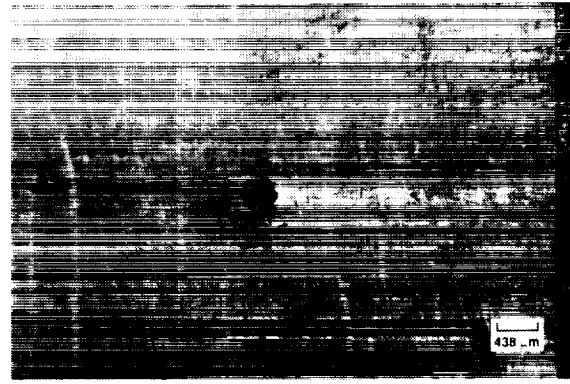Figure VI-11. Representative impacts in metal matrix composites
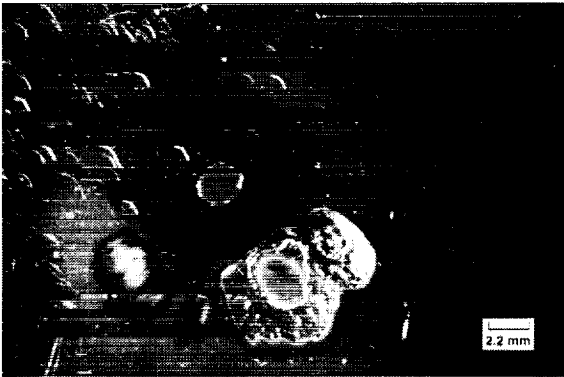
(a)

(b)

(c)

(d)

**LANDSCAPE**

Figure VI-12. Impacts in polymeric materials. a) leading-edge black RTV 602; b) trailing-edge black RTV 602; c) Tefzel strip; d) plastic-metal laminate.

402

(a)


(b)


(c)


(d)

**LANDSCAPE**

Figure VI-13. Impacts in metallized polymer films. a) and b) Silver-Teflon; c) and d) aluminized Kapton

## F. Paints

In addition to the examples of impact phenomenology of white thermal control paints already presented in this report, Figure VI-14 presents three examples of hypervelocity hits in other thermal control paints. In (a), Sperex 101, a silicone-based paint, on aluminum indicates melt and flow of both the paint and the substrate, which, for unknown reasons, was generally not seen with the S13GLO. A silicate-based paint, Z-93, on aluminum shown in (b) indicates localized damage with no melt or flow of either paint or substrate. Lastly, in (c), Chemglaze Z-306, a black thermal-control paint, sprayed over a brown primer on graphite epoxy is shown indicating more the response of the substrate rather than the paint.
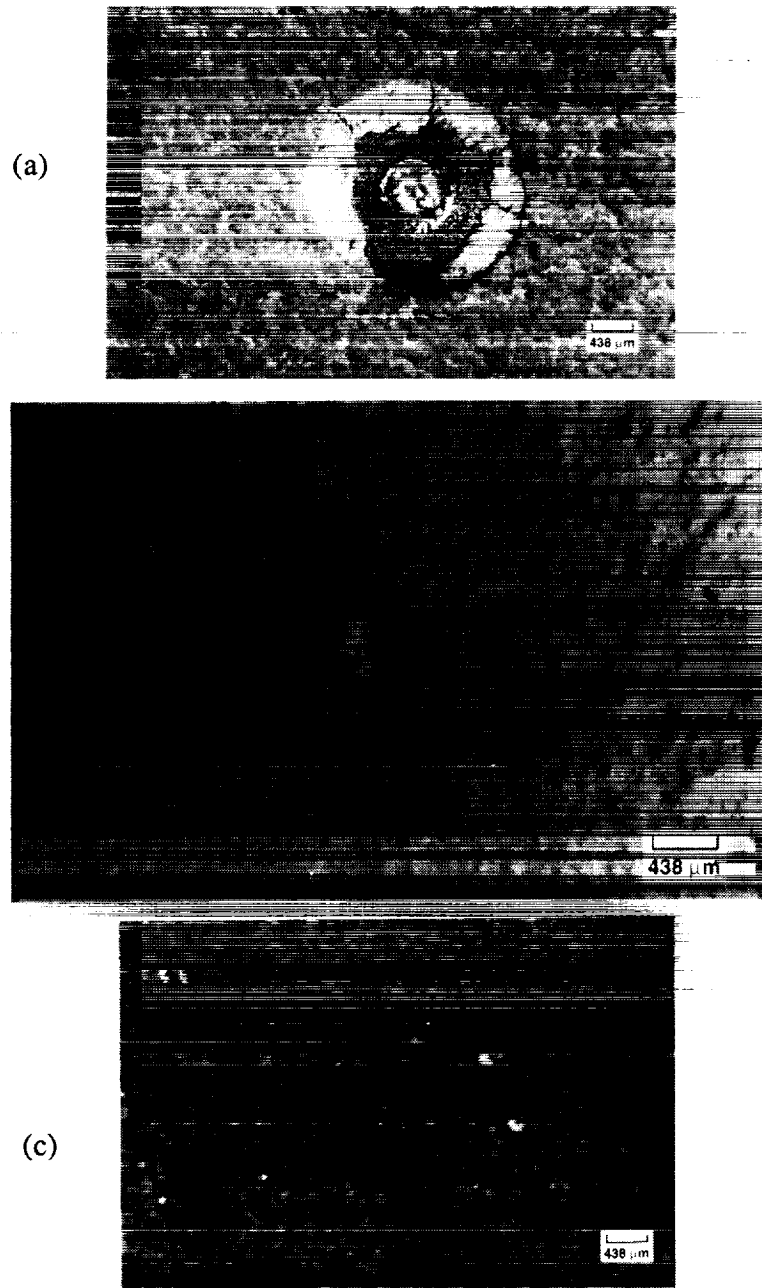
(a)

(b)

(c)

Figure VI-14. Impacts in miscellaneous paints: a) Sperex 101; b) IITRI Z-93; c) Chemglaze Z-306.

# VII.  COMPARISON TO CURRENT MODELS

The data from each surface was compared to currently accepted NASA models for space debris and micrometeoroids.  The models used for the analysis are the Orbital Debris Environment for Spacecraft of Kessler[12] and the Meteoroid Environment Model of Cour-Palais[19].  For the D8 surfaces, these two models, as well as their sum, were used for a comparison to the data.  The D4 surfaces are compared only to the meteoroid model since the debris model indicates several orders of magnitudes smaller fluxes relative to meteoroids for this surface of LDEF.  The obvious rationale for this is that due to the three-axis stabilization of LDEF, the leading edge should see both meteoroids and space debris, while, simplistically, the trailing edge will only be hit by meteoroids.  This is obviously an oversimplification since other LDEF data has indicated the importance of trailing edge impacts from space debris in elliptical orbits.[8,9]

The Kessler debris model[12] gives data on impactor hits per area versus impactor diameter.  However, the data from this study, and LDEF in general, is in the form of impactor hits per area versus crater diameter.  It therefore becomes necessary to relate impactor diameter to impactor crater diameter to translate these models so that this data can be compared to such predictions.  One method of simple conversion is based on the fact that for a given impactor size, the greater the impactor speed and the greater the impactor density, the larger will be the impactor crater.  Thus, a scaling law can be applied to relate the sizes of measured craters to the sizes of the impactors producing them.  This simple scaling method, known as the energy rule, involves a cube-root law of density ratios of the impactor to the target surface, and uses a two-thirds power law for the collision velocity.  The expression is normalized with a constant obtained from known terrestrial impact data of aluminum into aluminum.  The aluminum/aluminum constant is fairly appropriate for this and other LDEF data since the vast majority of impacts were into aluminum or coated-aluminum substrates.  The equation[20] is:

$$\frac{dc}{dp} = [k(P_p/P_t)^{1/3}]V^{2/3} ,$$

where $P_p$ is the particle density, $P_t$ is the target density, V is the collision speed, and k is a normalization constant for Al/Al impacts.  Other scaling laws could be used and differ in the exponents for density and/or velocity.  However, since all of these exponents are less than unity, the conversion of impactor diameters to crater diameters is relatively insensitive to changes in the scaling law.

For the Cour-Palais meteoroid model, a similar conversion must be made.  This correction makes use of the NASA-recommended micrometeoroid density to arrive at the ratio of crater size to impactor size.[19]  Both curves derived from these equations applied to these models were supplied by members of the LDEF Meteoroid and Debris Special Investigation Group.[21]

This data derived from the models is then plotted as crater density (in craters/cm^{2}) as a function of crater diameter (cm).  The plots are log-log and are integral sums.  That is, a point on the curve represents the number density of craters of a specific size and larger.  Meteoroid and debris models have been run for every surface of LDEF.[20]  However, we are only interested in the results for D4 and D8 in this study.  The derived curves for these two locations on LDEF are shown in Figures VII-1 and VII-2.  The data obtained in this study on crater counts are presented in Figures VII-3 through VII-11.  Figure VII-3 is a plot of the data

for the largest area surface with the highest number of counts, the D8 EPDS sunshield. Recall that this was a friable surface and should show evidence of more impacts than other surfaces. This data is overlaid on the two models, and in Figure VII-4 it is overlaid on a line representing the sum of these models. Similar plots for all D8 surfaces and their comparison to the models and their sums are given in Figures VII-5 and VII-6, respectively. Similar graphs were made for the D4 surfaces as well. Figures VII-7 and VII-8 present this data. As is evident from Figure VII-2, the contribution due to debris on D4 is vanishingly small, so that no sum graphs were necessary.

Crater densities on the eight panels surveyed were reported in craters/cm$^2$. The standard deviation of these measurements was calculated using Poisson statistics. Error calculation in this manner was valid since the crater distribution on the panels satisfied the basic Bernoulli conditions: namely a large number of events (impacts) distributed randomly over a large surface area. The standard deviation in the crater density would follow as the square root of the actual crater count divided by the surface area. Error bars in the accompanying figures are ± one standard deviation.

For the D8 surfaces (leading edge), the general trend of the data is more in line with the meteoroid model as opposed to the debris model. While the sum of these models gives as good or better fit to the data in the intermediate range, the rollover of the crater population below roughly 100 microns is not predicted by the debris model. For the D4 surfaces (trailing edge), the correlation of the data to the meteoroid model prediction is better; however, the same rolloff of the crater number density at small diameters is observed to be more pronounced than predicted by the model. This may be a consequence of small particles impacting primarily in the anodic oxide layer, which is harder and more dense than the aluminum substrate. This would produce correspondingly smaller craters and cause a leftward shift to the data points.

Inspection of the curves for the D8 surfaces reveals some additional trends. The anodized aluminum panels on the leading edge give nearly identical fits to the model, with marked deviation from the prediction lines at diameters of 300 microns and smaller. This deviation amounts to a factor of about 2 for craters with diameters in the 100-micron range. In contrast, the two painted panels gave very different distributions, presumably due to the different materials used in the paints (silicone vs. urethane), as well as the high degree of surface roughness present in the S13GLO paint. Generally, the models give over predictions when compared to the data obtained for this surface. For the EPDS sunshield, the correlation appears very good, except below 50 microns. The disturbing point about the D8 surfaces is the slope of the curves relative to the model predictions at large diameters. While statistically the data does not indicate this with certainty, the trend is obvious and may indicate a divergence between theory and experimental data.

For the D4 surfaces, the correlation between theory and experiment is much better. Examples of excellent correlation are provided by the anodized aluminum panels. The painted surfaces, however, still have a more pronounced rollover below 100 microns.
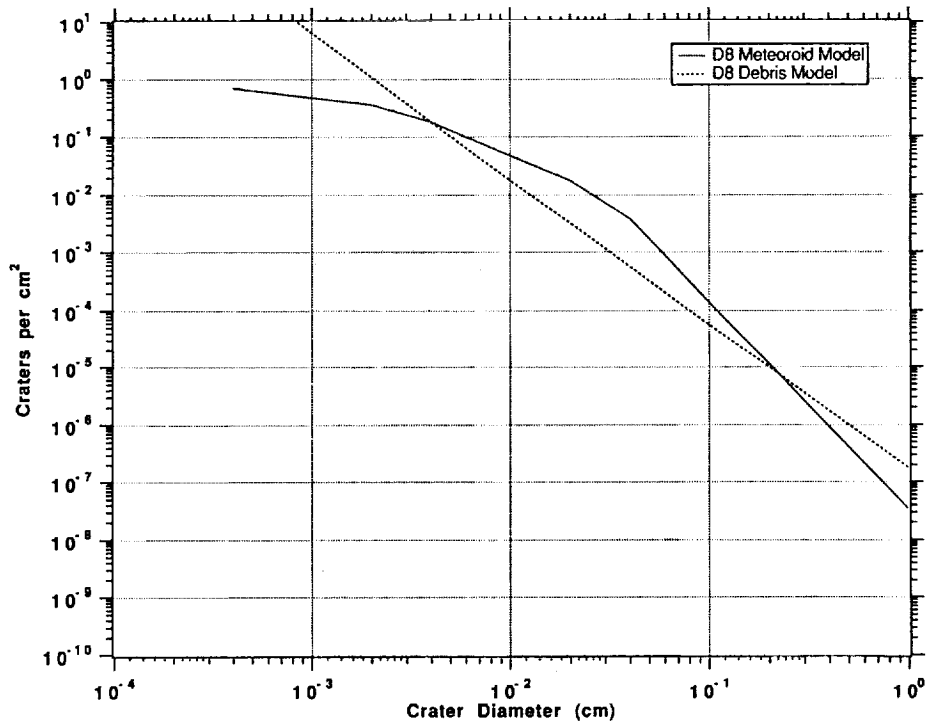
Figure VII-1. Meteoroid and Debris model predictions for LDEF row 8.*
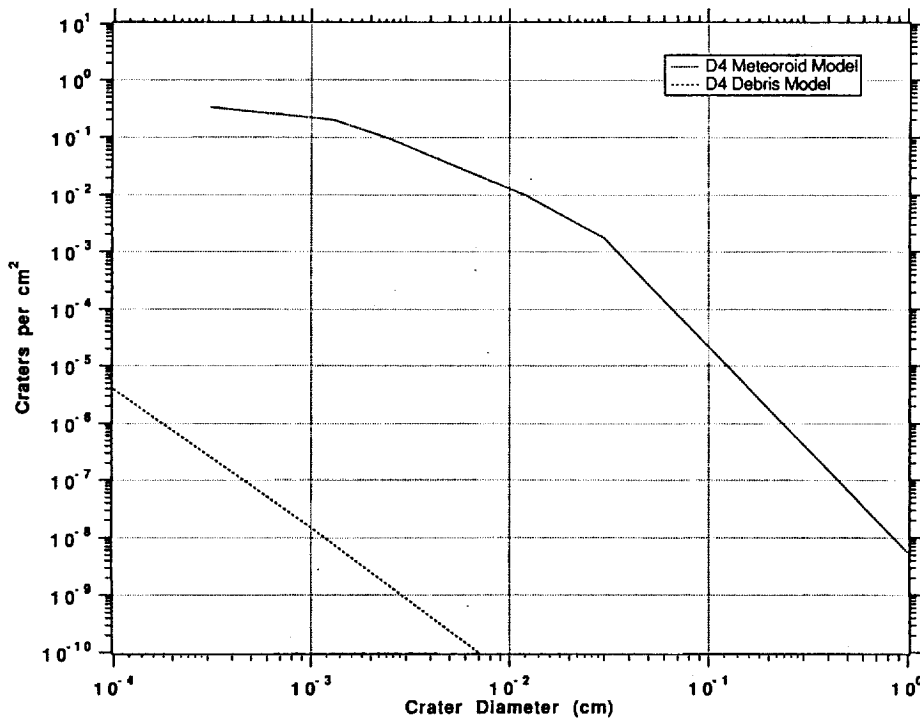


Figure VII-2. Meteoroid and Debris model predictions for LDEF row 4.*
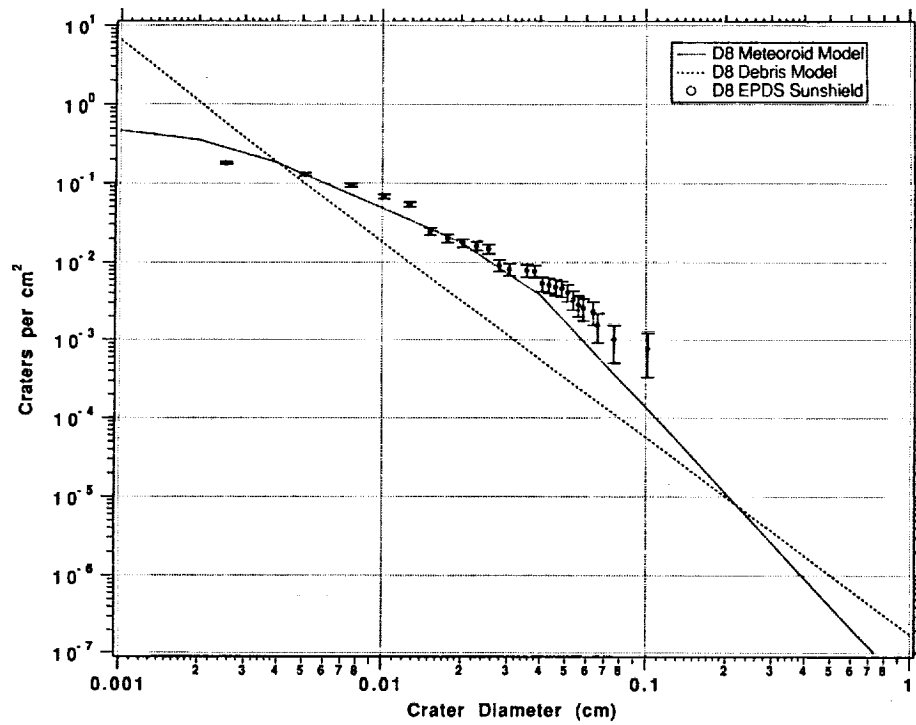
*D. R. Atkinson, private communication.

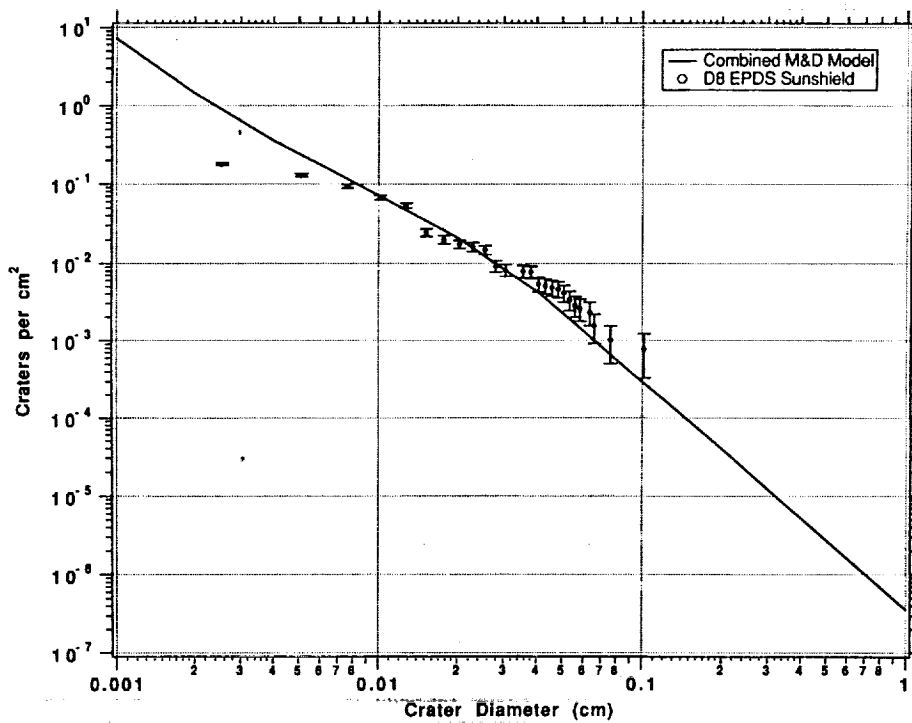Figure VII-3. D8 EPDS sunshield data compared to meteoroid/debris models.



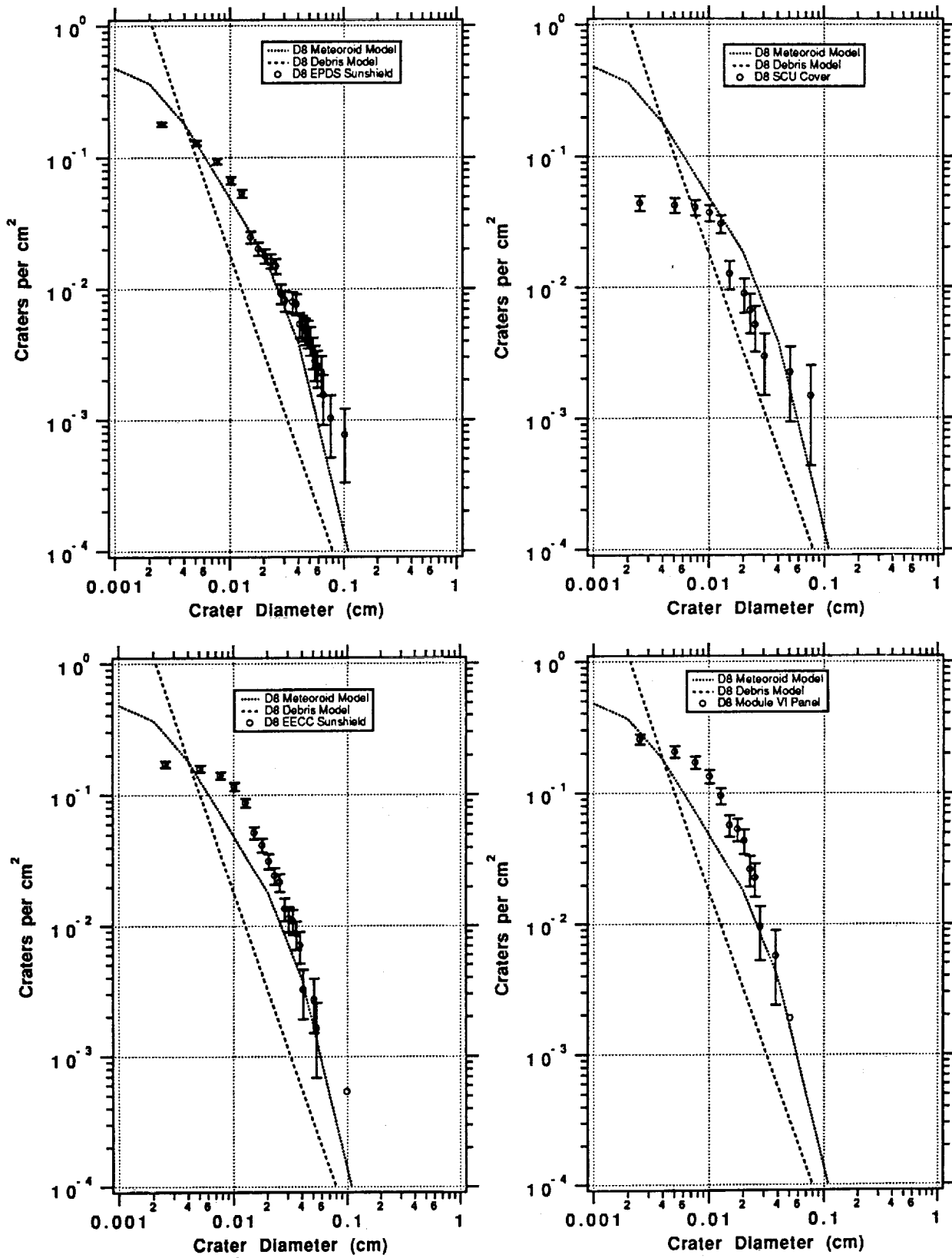Figure VII-4. D8 EPDS sunshield data compared to the sum of meteoroid and debris models.

408

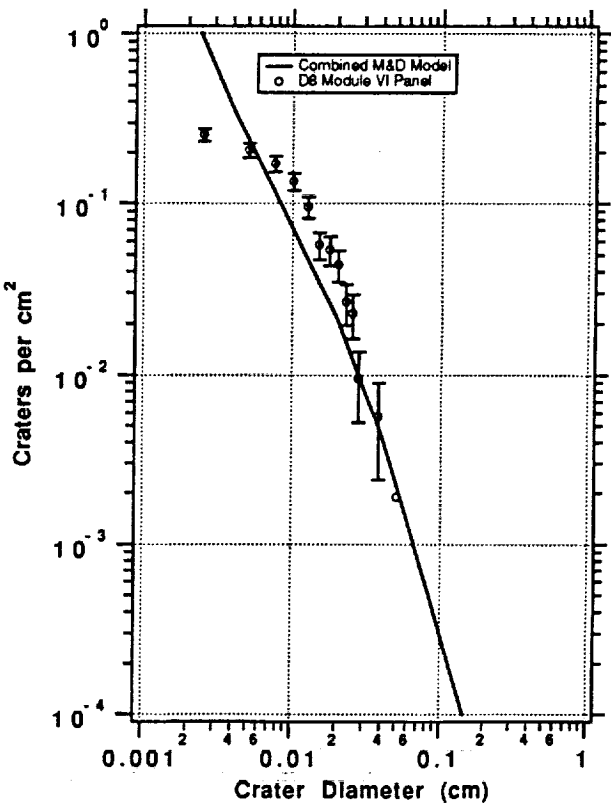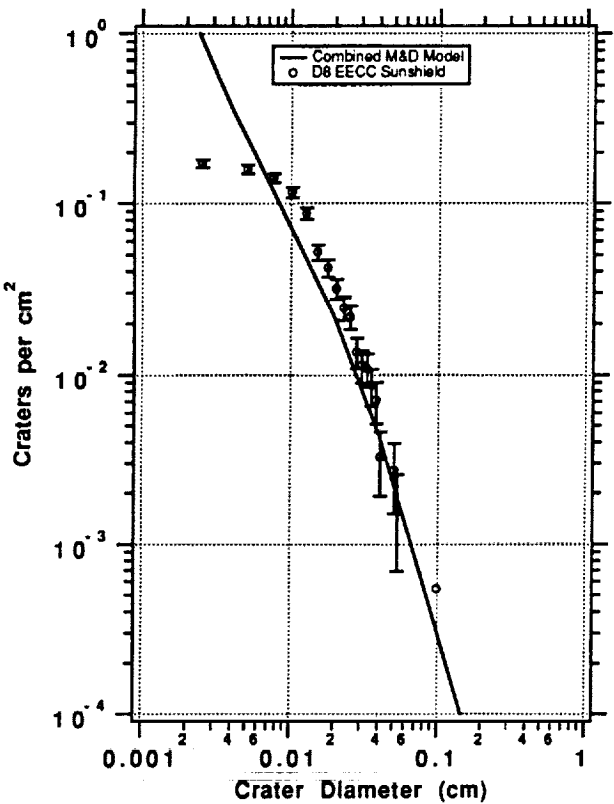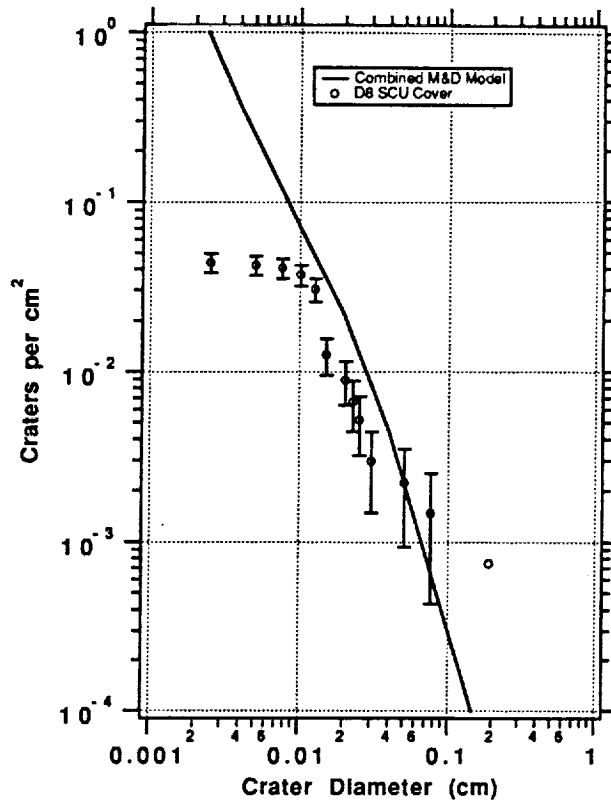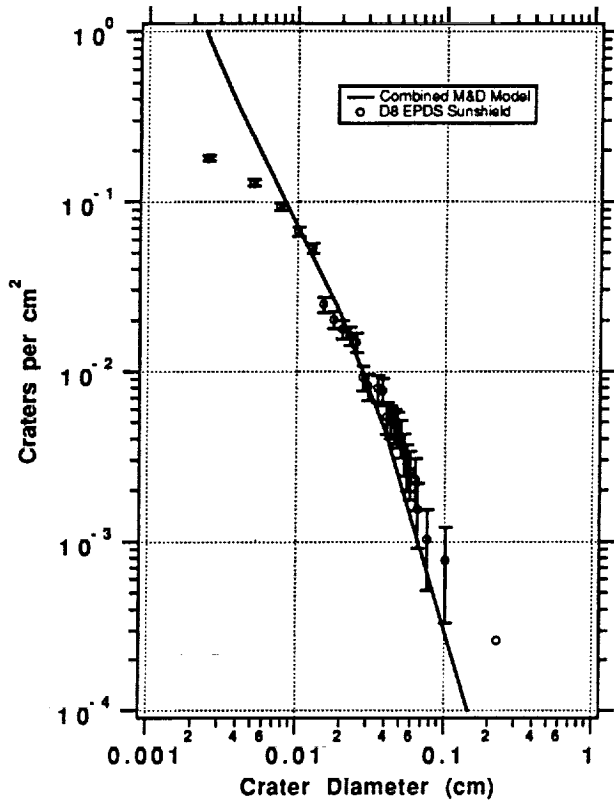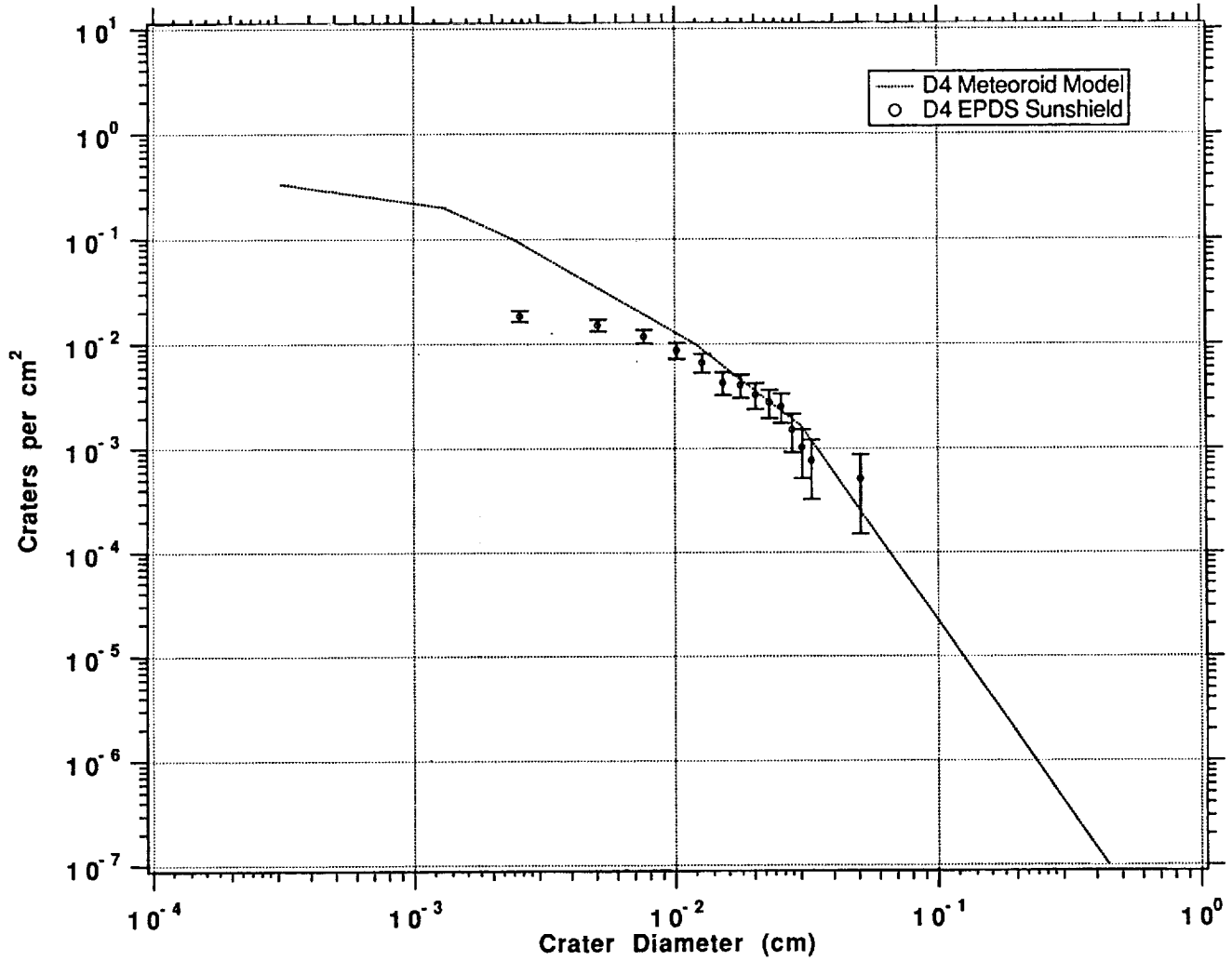Figure VII-5. Graphs for each D8 surface compared to models.

Figure VII-6.  Graphs of each  D8 surface compared to models' sums.

**LANDSCAPE**

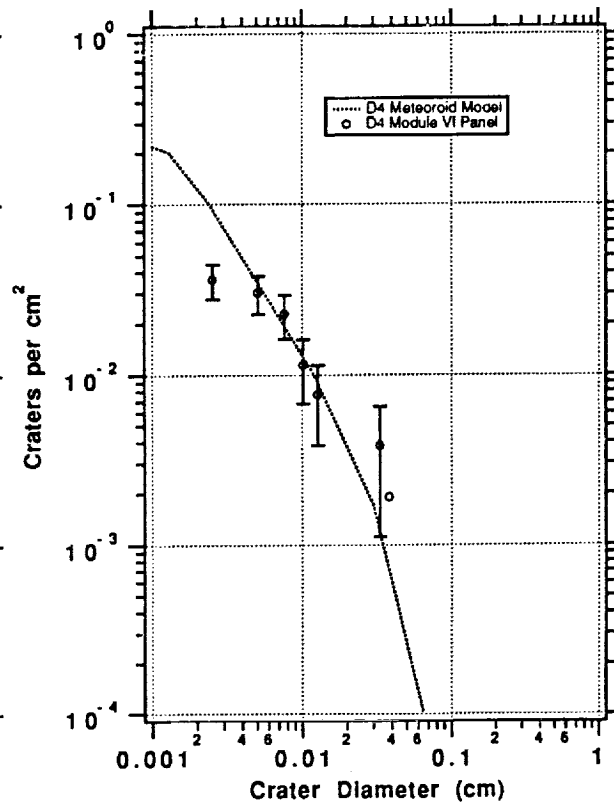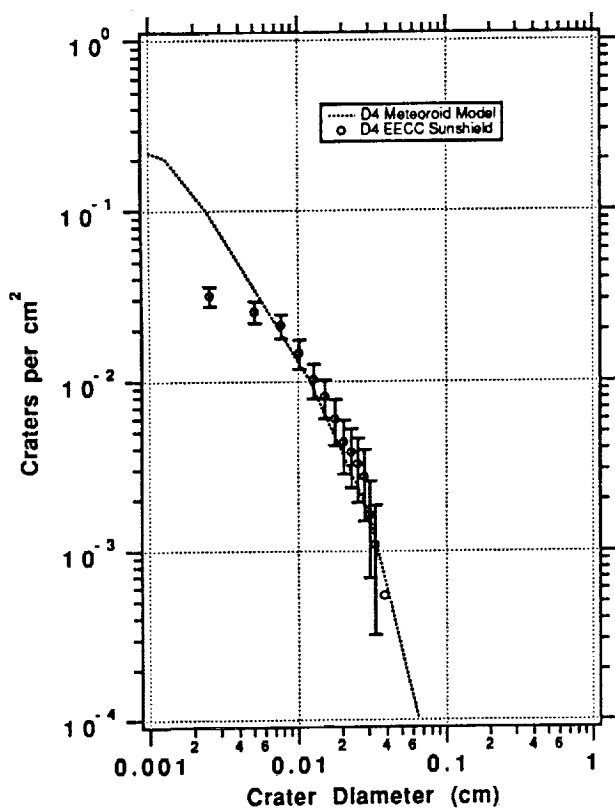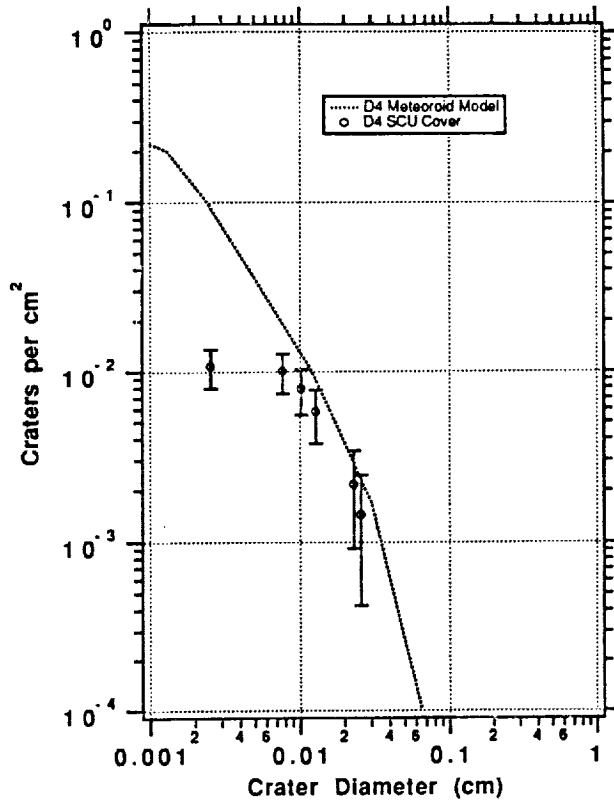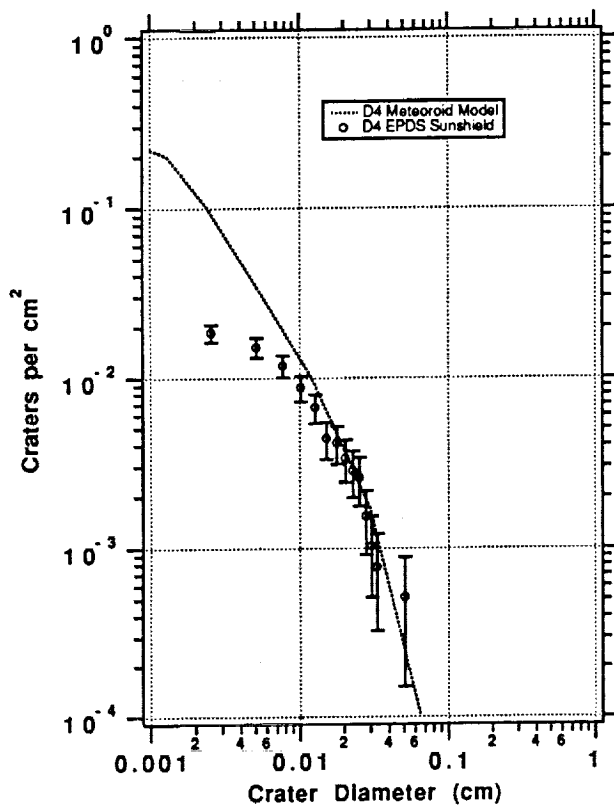Figure VII-7. D4 EPDS data compared to meteoroid model.

Figure VII-8. Graphs of each D4 surface compared to model.

# VIII. CONCLUSIONS

From the information and analysis presented in this and other reports, it becomes obvious that space debris, and to a lesser extent micrometeoroids, are increasing concerns for space systems reliability. Models that describe these environments have been developed and appear to do an adequate job for general predictions. Ground simulation facilities have also been developed that allow research in the area of material response to hypervelocity impact phenomena. Our experimental observations of the general response to these impacts of various material types, such as brittle or ductile materials, compare well to other experimental data both from flight experiments and ground simulations. While the damage to materials from hypervelocity impact phenomena as observed and documented on this experiment is not catastrophic, the effects of these phenomena on mission performance, especially for optical systems, needs to be studied further to allow better quantification of their associated risks.

Unique to LDEF is the observation of synergistic phenomena associated with micrometeoroid and debris impacts, especially due to atomic oxygen exposure. Such phenomena are among the more interesting aspects of LDEF, and they are beginning to become understood; however, more work is needed to fully understand, model, and simulate these events.

From this work, it is concluded that current models for space debris and micrometeoroids have limited accuracy over wide ranges of impactor diameters. Whether or not this limited accuracy is good enough for predicting design lifetimes of 15 to 30 years is still a point of contention. Clearly, the data from this study correlates with predictions better for the D4 surfaces as opposed to the D8 surfaces, which indicates that there are difficulties associated with prediction of ram impactor densities from either separate or summed models. There is a marked tendency to over predict the impactor density with diameters smaller than 0.01 cm (100 microns). While this is not a serious problem from a spacecraft designer's perspective, it may indicate a basic problem with the current models.

From the data in this study, it would appear that the number density of small impactors levels off instead of increasing as predicted by the models. Higher populations of small-diameter impactors were observed on the Interplanetary Dust Experiment, but this may be due to non-steady-state fluxes seen during the first year of the mission since the active data indicates a higher impact count than that determined passively after LDEF recovery.[9] Except for the S13GLO painted surfaces, which were quite rough, the surface texture of the panels surveyed was smooth enough to allow accurate counts of the number density of impacts, and, therefore, we believe the leveling-off of impactor density is real and not an artifact. Clearly, the response of painted and coated aluminum substrates differs from that of uncoated aluminum, and this is not taken into account by current models. This contributes to the observed rollover at small diameters.

A potentially more serious discrepancy with accepted models occurs at larger diameter impacts where the slope of the curves for the experimental data and those for the models visibly diverges and thus indicates a tendency towards underprediction. In some cases, the number of craters is statistically quite small, and, therefore, this conclusion needs to be approached with caution. However, we believe that this points to a need to update these models in the light of the singularly enormous amount of data obtained from LDEF.

## REFERENCES

1. T. H. See, M. A. Allbrooks, D. R. Atkinson, C. G. Simon and M. Zolensky, "Meteoroid and Debris Impact Features Documented on the Long Duration Exposure Facility, A Preliminary Report," *Planetary Science Branch Publication #84*, JSC #24608, August 1990.

2. For a description of LDEF and its experiments and environments see:

   R. L. O'Neal and E. B. Lightner, "Long Duration Exposure Facility-- A General Overview", LDEF-- 69 Months in Space First Post-Retrieval Symposium, NASA Conference Publication 3134 1992.

   W. H. Kinard and G. D. Martin, "Long Duration Exposure Facility (LDEF) Space Environments Overview", ibid.

3. D. H. Humes, "Large Craters on the Meteoroid and Space Debris Impact Experiment," ibid.

4. J. C. Mandeville and J. Borg, "Study of Dust Particles On Board LDEF, The Frecopa Experiments AO138-1 and AO138-2," ibid.

5. M. Finkenor, "Meteoroid and Debris Impacts on MSFC LDEF Experiments," ibid.

6. J. M. McDonnell and T. J. Stevenson, "Hypervelocity Impact Microfoil Perforations in the LEO Space Environment (LDEF, MAP AO023 Experiment)," ibid.

7. T. H. See, F. Horz, M. E. Zolensky, M. K. Allbrooks, D. R. Atkinson, and C. G. Simon, "Meteoroid and Debris Special Investigation Group Preliminary Results: Size Frequency Distribution and Spatial Density of Large Impact Features on LDEF," ibid.

8. F. Horz, R. P. Bernhard, J. Warren, T. H. See, D. E. Brownlee, M. R. Lawrence, S. Messenger and R. B. Peterson, "Preliminary Analysis of LDEF Experiment A0187-1: Chemistry of Micrometeoroids Experiment," ibid.

9. J. D. Mulholland, S. F. Singer, J. P. Oliver, J. L. Weinberg, W. J. Crooke, N. L. Montague, J. J. Wortman, P. L. Kassel and W. H. Kinard, "IDE Spatio-Temporal Impact Fluxes and High Time Resolution Studies of Multi-Impact Events and Long-Lived Debris Clouds," ibid.

10. C. G. Simon, J. L. Hunter, J. J. Wortman, and D. P. Griffis, "Ion Microprobe Elemental Analysis on Interplanetary Dust Experiment Sensor Surfaces," ibid.

11. H. A. Zook, "Deriving the Velocity Distribution of Meteoroids From the Measured Meteoroid Impact Directionality on the Various LDEF Surfaces," ibid.

12. D. J. Kessler, R. C. Reynolds, and P. D. Anz-Meador, "Orbital Debris Environment for Spacecraft Designed to Operate in Low Earth Orbit", *NASA -TM-100471*, September 1, 1988.

13. H. A. Zook, "Flux Versus Direction of Impacts on LDEF by Meteoroids and Orbital Debris," *Lunar and Planetary Science XXI*, 1990.

14. H. A. Zook, "The Velocity Distribution and Angular Directionality of Meteoroids that Impact on an Earth-Orbiting Satellite," *Lunar and Planetary Science Conference XVII Abstracts*, 1138-1139, 1987.

15. J. E. Erickson, "Velocity Distribution of Sporadic Photographic Meteors," *Journal of Geophysical Research*, *vol. 7, no. 12, 3721-3726, 1968.*

16. P. N. Peters and J. C. Gregory, "Pinhole Cameras as Sensors for Atomic Oxygen in Orbit; Application to Attitude Determination of LDEF", ibid.

17. M. J. Meshishnek, S. R. Gyetyay, and C. H. Jaggers, "Long Duration Exposure Facility Experiment M0003 Deintegration/ Findings and Impacts", *NASA Conference Publication 3134*, Part 2, 1073 1992.

18. S. R. Gyetvay, H. K. A. Kan, M. J. Meshishnek and J. M. Coggi, *M0003 Data Base Guide Book*, The Aerospace Corporation .

19. B. G. Cour-Palais et al., "Meteoroid Environment Model - 1969 (Near Earth to Lunar Surface)", *NASA SP-8013*, March 1969.

20. D. Atkinson, A Watts, and L. Crowell, "Spacecraft Microparticle Impact Flux Definition", UCRL-CR-108788, August 30, 1991.